



# Evolution of winter precipitation in the Nile river watershed since the last glacial

Vera Dorothee Meyer<sup>1</sup>, Jürgen Pätzold<sup>1</sup>, Gesine Mollenhauer<sup>1,2</sup>, Isla S. Castañeda<sup>3</sup>, Stefan Schouten<sup>4</sup>, and Enno Schefuß<sup>1</sup>

<sup>1</sup>MARUM – Center for Environmental Sciences, University of Bremen, 28359 Bremen, Germany

<sup>2</sup>Alfred Wegener Institute, Helmholtz Centre for Polar and Marine Research, 27570 Bremerhaven, Germany

<sup>3</sup>Department of Earth, Geographic and Climate Science, University of Massachusetts Amherst, Amherst, MA, USA

<sup>4</sup>Department of Marine Microbiology and Biogeochemistry, NIOZ Royal Netherlands Institute for Sea Research, 1790 AB Den Burg, the Netherlands

**Correspondence:** Vera Dorothee Meyer (vmeyer@marum.de) and Enno Schefuß (eschefuss@marum.de)

Received: 17 April 2023 – Discussion started: 27 April 2023

Revised: 13 December 2023 – Accepted: 20 December 2023 – Published: 14 March 2024

**Abstract.** Between 14.5 and 5 ka, the Sahara was vegetated owing to a wet climate during the African humid period. However, the climatic factors sustaining the “green Sahara” are still a matter of debate. Particularly the role of winter precipitation is poorly understood. Using the stable hydrogen isotopic composition ( $\delta\text{D}$ , where D stands for deuterium) of high molecular weight (HMW) *n*-alkanoic acids in a marine sediment core from the eastern Mediterranean, we provide a continuous record for winter precipitation in the Nile river delta spanning the past 18 kyr. Pairing the data with  $\delta\text{D}$  records from HMW *n*-alkanes from the same core, we show that HMW *n*-alkanoic acids constantly derived from the delta, while the HMW *n*-alkanes also received significant contributions from the headwaters between  $\sim 15$ –1 ka when fluvial runoff enhanced. This enables us to reconstruct the evolution of Mediterranean (winter) and monsoonal (summer) rainfall in the Nile river watershed in parallel. In the delta, the Heinrich stadial 1 (HS1) evolved in two phases, with a dry episode between  $\sim 17.5$ –16.0 ka, followed by wet conditions between  $\sim 16$ –14.5 ka. Winter rainfall enhanced substantially between 11–6 ka, lagging behind the intensification of the summer monsoon by ca. 3 kyr. Heavy winter rainfall resulted from a southern position of the Atlantic storm track combined with elevated sea surface temperatures in the eastern Mediterranean, reinforcing local cyclogenesis. We show that during the green Sahara, monsoon precipitation and Mediterranean winter rainfall were both enhanced and infer that the winter rainfall zone extended southwards,

delivering moisture to the Sahara. Our findings corroborate recent hypotheses suggesting that winter rains that extended southward were a crucial addition to the northward displacement of the summer monsoon in helping to sustain a green Sahara.

## 1 Introduction

Northern Africa underwent dramatic oscillations between dry and wet climate states during glacial–interglacial cycles (e.g., deMenocal et al., 2000a; Menviel et al., 2021; Larrasoña et al., 2013; Ziegler et al., 2010). The last wet phase occurred between 14.5–5 ka, reaching its climax between 11–6 ka (e.g., deMenocal et al., 2000a; Shannahan et al., 2015; Tierney et al., 2017; Dupont and Schefuß, 2018). At this time, which is known as the African humid period (AHP), humid conditions in northern Africa transformed the formerly barren, hyperarid Sahara desert into a fertile “green Sahara” ( $\sim 11.5$ –5 ka; Kuper and Kröpelin, 2006) where savannah, lakes, rivers and wetlands existed, allowing human settlements in the Sahara (Kuper and Kröpelin, 2006; Quade et al., 2018; Larrasoña et al., 2013; Jolly et al., 1998). Although intensively studied, the drivers and spatiotemporal extent of the AHP are still a matter of debate (Lüning and Vahrenholt, 2019; Kutzbach et al., 2014; Otto-Bliesner et al., 2014; Menviel et al., 2021; Tierney et al., 2017; Sha et al., 2019; Cheddadi et al., 2021). There is consensus that the

AHP was initiated in response to insolation forcing, which intensified the African summer monsoon and shifted the Intertropical Convergence Zone (ITCZ) and the African rainbelt northward (Menviel et al., 2021; Lüning and Vahrenholt, 2019; Pausata et al., 2016; Braconnot et al., 2007; Claussen et al., 2017; deMenocal et al., 2000b). Next to orbital forcing, positive non-linear feedbacks from the land surface amplified the climatic changes (e.g., Chandan and Peltier, 2020; Pausata et al., 2016, 2020).

Controversy exists on the termination of the AHP (Kuper and Kröpelin, 2006; Shannahan et al., 2015; Schefuß et al., 2005; Costa et al., 2014; Blanchet et al., 2014; deMenocal et al., 2000a; Tierney and deMenocal, 2013; Ménot et al., 2020; Tierney et al., 2008; Berke et al., 2012; Weldeab et al., 2014; Junginger et al., 2014; Castañeda et al., 2016a; deMenocal, 2015; Collins et al., 2017), as well as on the climatic processes sustaining a vegetated Sahara (Cheddadi et al., 2021; Kutzbach et al., 2014; Alpert et al., 2006; Chandan et al., 2020; Braconnot et al., 2007; Hopcroft et al., 2017; Claussen et al., 2017; Sha et al., 2019; Tierney et al., 2017). Paleoclimate records suggest both a gradual and an abrupt ending of the AHP and indicate that the AHP terminated earlier in the north than in the south (Kuper and Kröpelin, 2006; Shannahan et al., 2015; deMenocal, 2015). For a long time, most studies focused on the northward extension of the summer monsoon, seeking to explain the AHP and the green Sahara (deMenocal et al., 2006b; Braconnot et al., 2007; Menviel et al., 2021; deMenocal et al., 2000b; Shannahan et al., 2015; Sha et al., 2019; Tierney et al., 2017). However, reproducing the AHP and the green Sahara has challenged climate modelers for a long time because of inconsistencies between model results and proxy data, a problem that has not been overcome yet (Chandan and Peltier, 2020; Braconnot et al., 2007; Hopcroft et al., 2017; Perez-Sanz et al., 2014; Thompson et al., 2019, 2021). Modern simulations combining orbital forcing and land–surface feedbacks tend to underestimate rainfall amount inferred from pollen and leaf wax isotopic compositions between 25–31°N (Chandan and Peltier, 2020; Thompson et al., 2019, 2021).

Given these inconsistencies, contributions from additional moisture sources such as the Mediterranean winter rains increasingly receive attention to explain the green Sahara (Kutzbach et al., 2014; Cheddadi et al., 2021; Tierney et al., 2017).

Recently, Cheddadi et al. (2021) suggested that intensified Mediterranean winter rainfall and a southward extension of the winter rainfall zone into the Sahara may have delivered the additional moisture needed for sustaining a green Sahara by decreasing rainfall seasonality. Beforehand, Tierney et al. (2017) had already invoked additional winter precipitation to fully explain their observed amplitude in precipitation records from northwestern Africa. A model-based investigation of the response of Mediterranean winter rainfall confirms intensified precipitation in northern Africa and the

Middle East during the AHP in response to orbital forcing (Kutzbach et al., 2014).

Unfortunately, the glacial-to-Holocene development of winter precipitation in northeastern Africa remains elusive, given the scarcity of proxy records. To improve the understanding of how winter and summer precipitation evolved around the AHP, continuous records for precipitation are required to robustly investigate spatial variations in rainfall across northern Africa. Constraints on the hydroclimatic development in the southeastern Mediterranean come from Earth system models and various paleoenvironmental archives from the Asian borderlands of the Levantine Basin (Langgut et al., 2016; Tierney et al., 2022; Stein, 2001; Ludwig and Hochmann, 2022; Bar-Matthews et al., 1997; Goldsmith et al., 2017; Enzel et al., 2008; Cheng et al., 2015; Miebach et al., 2019).

While there is consensus that during the Last Glacial Maximum (LGM) the eastern Mediterranean realm was characterized by a more positive moisture balance (Stein, 2001; Goldsmith et al., 2017; Ludwig and Hochmann, 2022), the effects from changes in evaporation and precipitation on effective moisture are still debated. Some authors proposed increased precipitation (Enzel et al., 2008; Stein et al., 1997; Cheng et al., 2015), while others suggested reduced precipitation (Ludwig and Hochmann, 2022; Bar-Matthews et al., 1997; Langgut et al., 2021). While the sign of rainfall changes is ambiguous, there is a broad consensus among proxy data and model results that evaporation was lower under cold glacial conditions (Stein, 2001; Tierney et al., 2022; Ludwig and Hochmann, 2022; Goldsmith et al., 2017). These uncertainties in terms of rainfall ask for more studies to address the hydroclimate development in the eastern Mediterranean since the LGM.

A key region to study northeastern African climate change is the Nile river basin that extends over 3 million km<sup>2</sup> (Fig. 1). Currently, the Nile river basin is influenced by monsoonal summer rains south of the Sahara desert and Mediterranean winter rainfall in the delta region. Furthermore, it is of societal relevance to address the climatic history of the Nile river catchment because the river is the lifeline of Egypt, providing fertile ground and drinking water to millions of people. It also played a vital role in the rise and demise of ancient Egyptian civilizations (e.g., Zaki et al., 2021). In northeastern Africa and the borderlands of the southern Levantine Basin, socioeconomic impacts due to increasing aridity are expected with future warming. Continuous archives for precipitation are predominantly found in the headwaters of the Nile river and further south (lakes Victoria, Tana and Tanganyika; Fig. 1; Berke et al., 2012; Costa et al., 2014; Tierney et al., 2008, 2010). In the northern part of the catchment where the hyperarid Sahara desert extends, continuous records for precipitation are sparse, as sedimentary sequences from the deglaciation and the Holocene, such as lacustrine deposits, were subject to strong wind erosion dur-

ing arid periods (Hamdan et al., 2016; Hamdan and Lucarini, 2013).

Sediment cores from the Levantine Basin (Fig. 1) are used to reconstruct environmental changes in the Nile river watershed. These records are commonly considered to be integrators of the entire catchment and are mostly interpreted to reflect monsoonal rainfall variability (Castañeda et al., 2016a; Revel et al., 2015; Ménot et al., 2020; Blanchet et al., 2014). However, the Nile crosses several climate regimes that drastically differ in precipitation amount and seasonality, including tropical conditions in the headwaters, hyperarid desert in its central part and Mediterranean winter rainfall in the delta region. For climate reconstructions, it is crucial to address these climate zones separately to identify latitudinal differences and to understand how monsoonal (summer) and Mediterranean (winter) precipitation evolved around the AHP.

Here, we provide a new hydroclimate record based on the stable hydrogen isotopic composition ( $\delta^2\text{H}$  or also often termed  $\delta\text{D}$ , where D stands for deuterium) of high molecular weight (HMW) *n*-alkanoic acids. HMW *n*-alkanoic acids are major components of epicuticular leaf waxes of higher plants (Eglinton and Hamilton, 1967). The record is obtained from marine sediment core GeoB7702-3 from the eastern Mediterranean Sea (Fig. 1).  $\delta\text{D}$  of leaf wax lipids ( $\delta\text{D}_{\text{wax}}$ ) is a powerful means to reconstruct past hydrological changes (e.g., Sachse et al., 2012) and has been successfully applied to infer hydroclimate variability across Africa (Schefuß et al., 2005; Tierney et al., 2008, 2017; Berke et al., 2012; Costa et al., 2014; Collins et al., 2013; Castañeda et al., 2016a; Konecky et al., 2011). We infer that  $\delta\text{D}_{\text{wax}}$  of our HMW *n*-alkanoic acids records winter precipitation in the Nile delta region. By comparison to existing  $\delta\text{D}_{\text{wax}}$  records based on HMW *n*-alkanes from the same core (Castañeda et al., 2016a) and HMW *n*-alkanoic-acid-based  $\delta\text{D}_{\text{wax}}$  records from the headwaters (Berke et al., 2012; Costa et al., 2014; Tierney et al., 2008), we are able to examine hydroclimate variability in the southern and northern sections of the Nile river catchment and shed light on the interplay of Mediterranean (winter) and monsoonal (summer) rainfall changes in northeastern Africa around the AHP.

## 2 Study area

Core GeoB7702-3 was recovered from the southeastern Levantine Basin off Israel (Fig. 1) (Pätzold et al., 2003). The core receives terrigenous material from the Nile river as the suspension load is transported eastward along the continental margin due to the counterclockwise direction of surface currents and eddies (e.g., Weldeab et al., 2002). This makes site GeoB7702-3 a suitable archive for environmental changes in the Nile river basin (Castañeda et al., 2010a, 2016a).

The Nile river is the longest river in the world, extending over  $34^\circ$  of latitude (Fig. 1). The catchment spans

from equatorial Africa to the Mediterranean coast draining Uganda, Ethiopia, South Sudan, Sudan and Egypt (Fig. 1). The river consists of three major tributaries, i.e., the White Nile (sourced from Lake Victoria); the Blue Nile (sourced from Lake Tana); and the Atbara River (the source is situated north of Lake Tana). The confluence of the three tributaries forms the main Nile (Fig. 1). For the following discussion, we define three sub-catchments of the watershed as follows: upper catchment (headwaters in Ethiopia and Uganda;  $15^\circ\text{N}$  to  $4^\circ\text{S}$ ); middle catchment (Sahara, Sudan and Egypt;  $15\text{--}30^\circ\text{N}$ ); and lower catchment (Nile delta;  $30\text{--}31^\circ\text{N}$ ). On its way to the north, the Nile river crosses different climate zones and vegetation regimes. The climate zones encompass a wet, tropical climate in Ethiopia and Uganda, the semi-arid Sahel zone, the hyperarid Sahara desert and Mediterranean climate in the delta region (e.g., Korecha and Barnston, 2007). The upper section of the watershed is characterized by heavy rainfall (e.g., about  $1874\text{ mm yr}^{-1}$  in Addis Ababa, Ethiopia; about  $1747\text{ mm yr}^{-1}$  in Kampala, Uganda). In Ethiopia, most rain falls between June and September. Uganda receives year-round precipitation with rainfall maxima during March until May and September until November. In the lower and middle catchment, rainfall mainly occurs during winter. In the Nile delta, annual rainfall spans from  $181\text{ mm yr}^{-1}$  along the coast (Alexandria) to  $18\text{ mm yr}^{-1}$  at its southern edge (Cairo). Most rain falls between October and March. Usually, the Sahara does not receive any rainfall (e.g., Luxor; <https://en.climate-data.org>, last access: 14 December 2022, AM Online Projects – Alexander Merkel, 2022a–e).

Precipitation in the upper Nile river watershed is mainly determined by the West African Monsoon and thus related to the seasonal migration of the ITCZ (Fig. 1). During the summer months, the seasonal northward movement transports moisture-laden air to southern northeastern Africa (up to  $\sim 15^\circ\text{N}$ ). Additionally, the Congo Air Boundary controls the relative contribution of moisture from the Gulf of Guinea, i.e., the Atlantic Ocean, and Indian Ocean to the headwaters (Fig. 1) (Camberlin, 2009). North of  $15^\circ\text{N}$ , the catchment is predominantly under the influence of the westerlies receiving moisture from the Atlantic Ocean and the Mediterranean Sea, the Arabian Peninsula and the Red Sea (Fig. 1) (Viste and Sortberg, 2013). The southern Mediterranean climate is characterized by dry summers and wet winters. Winter precipitation is governed by cyclogenesis over the eastern Mediterranean, so-called “Cyprus lows”. The cyclones form when relatively cold European air encounters the warm Mediterranean Sea during southward advection (Alpert et al., 1990). Next to the Cyprus lows, the Red Sea Trough is another local atmospheric circulation pattern controlling winter rainfall. It is commonly associated with warm and dry conditions but variations in its position can cause heavy precipitation events (Tsvieli and Zangvil, 2005; Krichak et al., 2012). The winter climate is largely dependent on teleconnections with the North Atlantic Oscillation (NAO), which

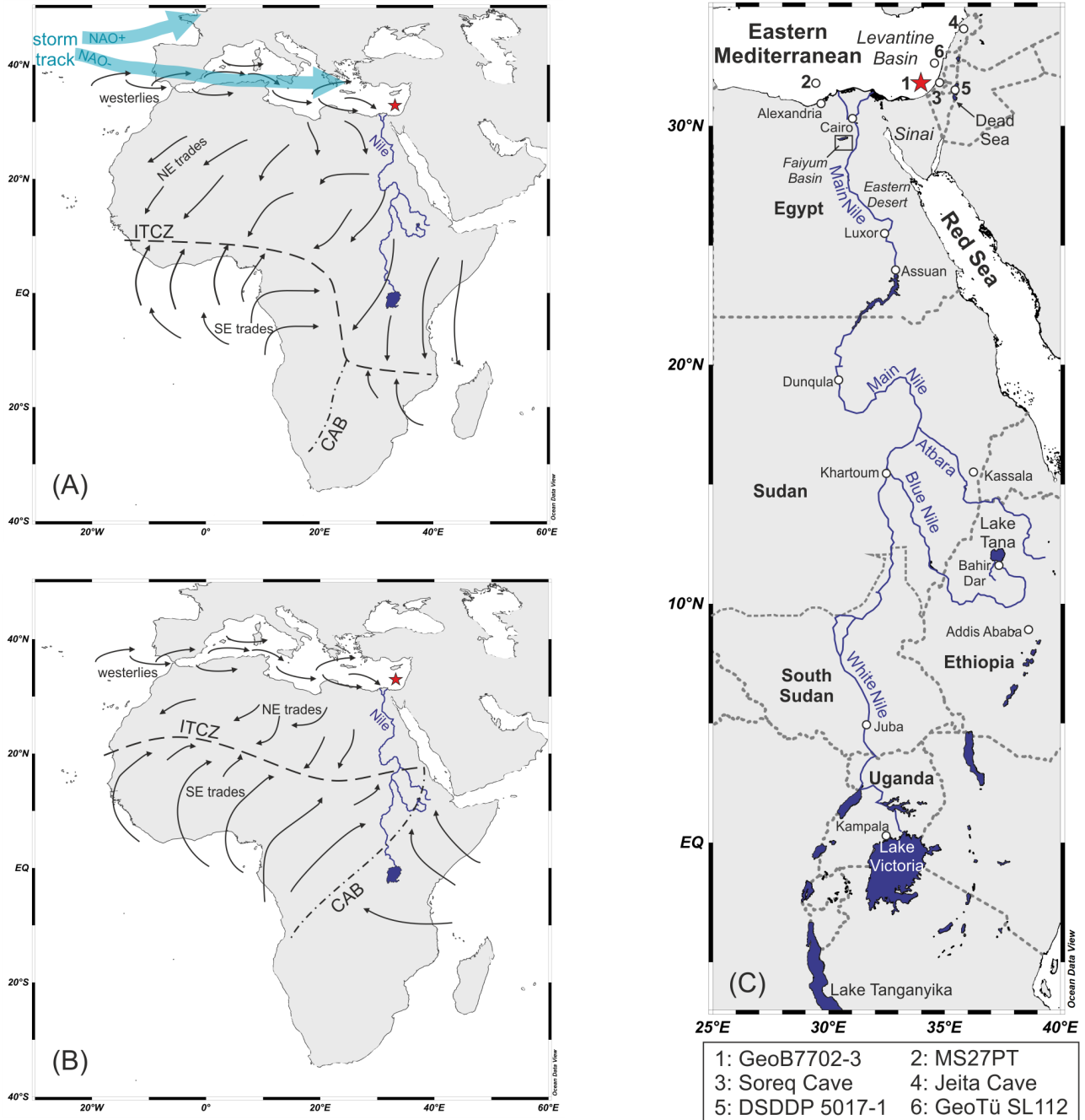


**Figure 1.** General wind patterns over Africa during winter (a) and summer (b). The red star marks site GeoB7702-3. The modern positions of the Intertropical Convergence Zone (ITCZ) and Congo Air Boundary (CAB) during January (a) and July/August (b) are sketched. (a) The positions of the North Atlantic storm track are marked for positive and negative phases of the North Atlantic Oscillation (NAO). (c) Detailed map of the Nile river watershed. Site GeoB7702-3 is marked by a red star. Other locations mentioned in the text are indicated by circles. The maps were created using Ocean Data View 5.6.3 (Schlitzer, 2006).

forms a constituent of the Arctic Oscillation. Modulating the positions of the Atlantic and Mediterranean storm tracks (Fig. 1), the NAO exerts strong control over moisture delivery to the Mediterranean borderlands. Warm and wet winters in the southern Mediterranean are generally associated with negative NAO states, while cold and dry winters occur during positive phases (Eshel and Farrel, 2000).

### 3 Material and methods

#### 3.1 Core material and chronology

Gravity core GeoB7702-3 was recovered from the continental slope off Israel at 562 m water depth during research vessel (RV) *Meteor* cruise M52/2 in 2002 (Pätzold et al., 2003). Prior to sampling, the core was stored at 4 °C. Age control for this core was previously established by Castañeda et al. (2010a) and is based on accelerator mass spectrometry (AMS) radiocarbon dates of planktic foraminifera. We refined the age model using up-to-date calibration curves and nine additional AMS dates (Table 1). To isolate foraminifera, the samples were wet-sieved, and specimens of the foraminifera *Globigerinoides ruber alba* were hand-picked from the 150–63 µm fraction. In cases where the abundance of *G. ruber* was insufficient, we mixed planktonic foraminifera species to obtain enough material (Table 1). In total, 290–810 µg carbon was dated at the MICADAS (Mini Carbon Dating System) AMS dating facility at the Alfred Wegener Institute, Helmholtz Centre for Polar and Marine Research (Bremerhaven, Germany), according to in-house protocols (Mollenhauer et al., 2021). The dates were combined with the data set of Castañeda et al. (2010a) to create the age–depth model. All radiocarbon dates are listed in Table 1. BACON 2.5.8 software (Blaauw and Christen, 2011) was used for age–depth modeling. Radiocarbon ages were transferred into calendar ages, based on the Marine20 calibration curve (Heaton et al., 2020). Today, the mean reservoir age offset ( $\Delta R$ ) in the Levantine Basin is  $-94 \pm 94$  years in relation to Marine20 (marine reservoir correction database; Reimer and Reimer, 2001). BACON was run with a constant  $\Delta R = -100 \pm 100$  years, accordingly. Default settings were used for the prior, apart from the accumulation rate, which was set to  $50 \text{ yr cm}^{-1}$ . BACON operated with 118 core slices. The age–depth model for GeoB7702-3 and the prior distributions are plotted in Fig. 2.

#### 3.2 Lipid extraction, quantification and isotopic analysis

For biomarker analyses, a total of 51 samples were collected every 5–12 cm, providing a mean temporal resolution of  $\sim 350$  years between samples. Target biomarkers of our study are HMW *n*-alkanoic acids and HMW *n*-alkanes and their stable isotope compositions. For the analysis of HMW *n*-alkanoic acids, the lipid extraction and isotopic analysis were performed at MARUM – Center for Marine Environ-

mental Sciences (University of Bremen, Germany). The sediment samples were freeze-dried and homogenized afterwards using a mortar and pestle. The soluble organic matter was extracted from  $\sim 5$  g of sediment using an Accelerated Solvent Extractor (ASE200). Extraction was performed with three cycles lasting 5 min each, using dichloromethane (DCM) : methanol (9 : 1 *v/v*) at 100 °C and 1000 psi. Then 19-methyl-arachidic acid was added to the samples as an internal standard prior to extraction. The total lipid extracts were saponified using potassium hydroxide (KOH). Neutral lipids and fatty acids were recovered using *n*-hexane and DCM, respectively. The fatty acids were methylated using methanol of known isotopic signature. The fatty acid methyl esters (FAMES) were cleaned by means of column chromatography. Columns consisted of 4 cm deactivated silica (1 % H<sub>2</sub>O in *n*-hexane) and 0.5 cm sodium sulfate (Na<sub>2</sub>SO<sub>4</sub>) in a Pasteur pipette with 5 mm diameter. FAMES were recovered using DCM : Hexane (2 : 1).

FAMES were quantified by gas chromatography and flame ionization detection (GC-FID) using a Thermo FOCUS GC. The GC was equipped with a Restek Rxi-5ms column. FAMES were analyzed using a similar method as in Gensel et al. (2022). For the quantification of the FAMES of HMW *n*-alkanoic acids, the response factors of the target compounds were determined from an external standard mixture containing five HMW *n*-alkanoic acid homologues (C<sub>24:0</sub>, C<sub>26:0</sub>, C<sub>28:0</sub>, C<sub>30:0</sub> and C<sub>32:0</sub>) at a concentration of 50 ng µL. The external standards were run every six samples. The relative standard deviation of the peak areas was  $> 9\%$ .

Isotope analysis of stable hydrogen ( $\delta D$ ) of the HMW *n*-alkanoic acids was performed using gas chromatography coupled to isotope ratio mass spectrometry (GC-IRMS). We used a Thermo Fisher Scientific TRACE™ GC coupled to a MAT 253 MS. Isotope values were measured against calibrated reference gas (H<sub>2</sub>). Values are reported in per mille relative to the Vienna Standard Mean Ocean Water (VSMOW) standards. A standard mixture consisting of 16 *n*-alkanes was run on every sixth sample to monitor the performance of the system. For the  $\delta D$  analysis, the accuracy and precision (mean deviation from offline values and the respective relative standard deviation, RSD) were 2.2‰ and 3.0‰, respectively. The instrument was operated only when the average absolute deviation from offline values was  $< 5\%$ . The H<sub>3</sub><sup>+</sup> factor was measured daily and was  $5.6 \pm 0.1$  throughout the measurement series. Replicate measurements of the samples yielded a standard deviation of 0.1‰–3.8‰ for  $\delta D$ .

We report the  $\delta D$  signatures of the *n*-C<sub>26:0</sub> and *n*-C<sub>28:0</sub> alkanolic acids, as they are the most abundant homologues in our samples. The  $\delta D$  of the respective FAMES were corrected for the bias introduced during the methylation process using isotope mass balance (hereafter  $\delta D_{\text{wax } n\text{-alkanoic acid}}$ ).  $\delta D_{\text{wax } n\text{-alkanoic acid}}$  was further corrected for deglacial changes in global ice volume applying stacked data of oxygen isotopic compositions ( $\delta^{18}\text{O}$ ) of benthic foraminifera (L04-stack; Lisiecki and Raymo, 2005) and

**Table 1.** List of AMS dates and corresponding calendar ages (cal. age) used to establish the age–depth model of GeoB7702-3. AMS dates were compiled from this study and Castañeda et al. (2010a, b). Samples from this study were dated at the MICADAS dating facility at Alfred Wegener Institute (Bremerhaven, Germany) while Castañeda et al. (2010a, b) performed dating at the Leibniz Laboratory for Radiometric Dating and Stable Isotope Research (Christian Albrechts University, Kiel, Germany). The age–depth model is based upon the median values of the calendar ages calculated.

Depth (cm)	Sample label	Dated material	AMS date ( $^{14}\text{C}$ a)	$2\sigma$ ( $\pm$ )	Cal. age min (a)	Cal. age max (a)	Cal. age median (cal a)	Cal. age mean (cal a)	Reference of AMS date
0	Set*	–	100*	10	64	124	98	97	This study
10	KIA25649	<i>G. ruber</i> and <i>O. universa</i>	245	30	123	415	221	231	Castañeda et al. (2010b)
64.5	KIA25648	<i>G. ruber</i> and <i>G. sacculifer</i>	1725	25	1086	1682	1342	1356	Castañeda et al. (2010b)
81.5–84.5	6279.2.1	<i>G. ruber</i>	2340	26	1615	2285	1929	1933	This study
102	KIA24619	<i>G. ruber</i>	2965	55	2288	2849	2580	2576	Castañeda et al. (2010b)
130–133	6281.1.1	<i>G. ruber</i>	3586	24	3113	3685	3400	3400	This study
132	KIA24617	<i>G. ruber</i>	3500	35	3189	3643	3413	3416	Castañeda et al. (2010b)
198–201	6277.2.1	<i>G. ruber</i>	5399	25	5353	6014	5697	5697	This study
210	KIA24616	<i>G. ruber</i>	5600	40	5764	6383	6036	6043	Castañeda et al. (2010b)
231–234	7307.1.1	<i>G. ruber</i>	7393	45	7242	8138	7724	7718	This study
242.5	KIA25646	<i>G. ruber</i> and <i>G. sacculifer</i>	7845	40	8023	8866	8327	8358	Castañeda et al. (2010b)
251–254	6280.1.1	<i>G. ruber</i>	9309	28	9015	10 110	9663	9652	This study
257	KIA24613	<i>G. ruber</i>	9070	60	9564	10 290	9934	9928	Castañeda et al. (2010b)
278–281	6276.2.1	Mixed planktonic foraminifera	10 144	34	11 051	12 047	11 502	11 508	This study
279	KIA24612	Mixed planktonic foraminifera	10 470	70	11 128	11 839	11 457	11 463	Castañeda et al. (2010b)
297–300	6275.2.1	<i>G. ruber</i>	11 827	32	12 688	13 729	13 215	13 213	This study
310	KIA24611	Mixed planktonic foraminifera	12 580	80	13 593	14 509	14 035	14 037	Castañeda et al. (2010b)
356	KIA24609	<i>G. ruber</i>	14 130	100	16 073	16 781	16 432	16 431	Castañeda et al. (2010b)
359–362	6274.2.1	<i>G. ruber</i>	14 420	37	16 264	17 074	16 666	16 664	This study
391	KIA24608	<i>G. ruber</i>	15 830	120	17 610	18 515	18 036	18 048	Castañeda et al. (2010b)
393–396	6262.2.1	<i>G. ruber</i>	15 275	39	17 690	18 728	18 151	18 176	This study
452	KIA25652	<i>G. ruber</i>	18 810	150	21 025	22 260	21 750	21 717	Castañeda et al. (2010b)
497	KIA24605	<i>G. ruber</i>	20 660	180	23 106	24 215	23 747	23 716	Castañeda et al. (2010b)
540.5	KIA24604	<i>G. ruber</i>	21 840	220	24 579	25 711	25 192	25 179	Castañeda et al. (2010b)
581.5	KIA25653	Mixed planktonic foraminifera	22 230	190	25 715	27 340	26 397	26 436	Castañeda et al. (2010b)

\* The core-top age was defined as 100 calendar ages in order to guarantee BACON calculates positive dates for the depths above the first AMS date (i.e., 10 cm).

the approach described in Ruan et al. (2019). We additionally analyzed the stable carbon isotopic composition of HMW *n*-alkanoic acids ( $\delta^{13}\text{C}_{\text{wax } n\text{-alkanoic acids}}$ ), as described in the Supplement (Sect. S1).

Prior to this study, a separate set of samples from GeoB7702-3 was extracted at the Royal Netherlands Institute for Sea Research (NIOZ) (Castañeda et al., 2010a). As described in Castañeda et al. (2016a), neutral lipids were split in apolar, keto and polar fractions by alumina oxide column chromatography with the following solvent mixtures: hexane : dichloromethane (9 : 1 *v/v*), hexane : DCM (1 : 1 *v/v*) and DCM : methanol (1 : 1 *v/v*). The apolar hydrocarbon fraction was further separated into saturated and unsaturated compounds using silica gel coated with silver nitrate ( $\text{AgNO}_3$ ). Identification of *n*-alkanes was performed on a Thermo Scientific Finnigan Trace Gas Chromatograph (GC) Ultra coupled to Thermo Scientific Finnigan DSQ mass spectrometer (MS) using a CP-Sil 5 fused silica capillary column (25 m  $\times$  0.32 mm; film thickness 0.12  $\mu\text{m}$ ) with helium as the carrier gas. Mass scans were made from *m/z* 50 to 800, with three scans per second and an ionization energy of 70 eV. The oven program started at 70  $^\circ\text{C}$ , increased by 20  $^\circ\text{C min}^{-1}$  to 130  $^\circ\text{C}$  and subsequently by a rate of

4  $^\circ\text{C min}^{-1}$  until 320  $^\circ\text{C}$  (held for 10 min). Quantification of *n*-alkanes was performed on an HP 6890 gas chromatograph (GC) using a 50 m CP Sil 5 column (0.32 mm diameter and 0.12  $\mu\text{m}$  film thickness) and helium as the carrier gas, with the same oven temperature program as for GC-MS. Compound concentrations were determined by relating chromatogram peak areas to the concentration of an internal standard of known concentration. Details regarding hydrogen and carbon isotopic analyses of the *n*-C<sub>29</sub> and *n*-C<sub>31</sub> alkanes are reported by Castañeda et al. (2016a).

Note that the set of samples taken for HMW *n*-alkanoic acids (this study) are at different sampling depths from the HMW *n*-alkanes (Castañeda et al., 2016a).

## 4 Results

### 4.1 concentrations of HMW *n*-alkanoic acids and HMW *n*-alkanes

Concentrations of HMW *n*-alkanoic acids are slightly lower during the early deglaciation (between 18–17 ka) than during the late Holocene (Fig. 3c). At  $\sim$ 16.5 ka, they decrease to a minimum. From 14.6 ka onwards, the contents

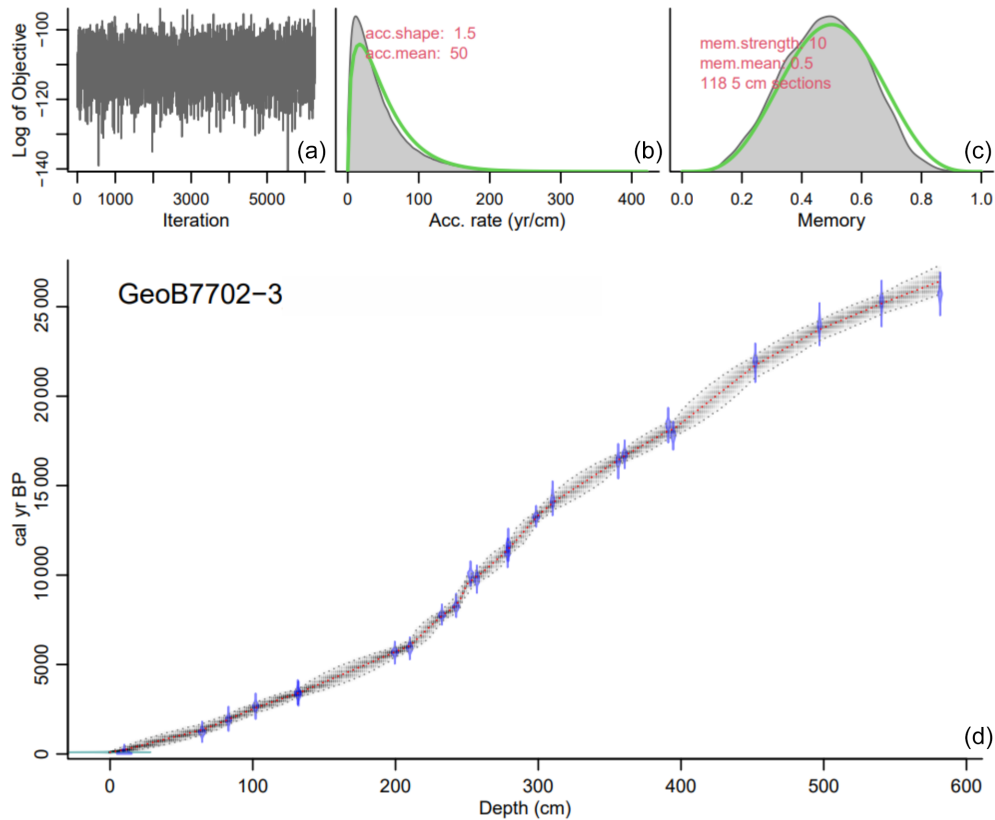


**Figure 2.** Output graph for the age–depth modeling approach for core GeoB7702-3 using the BACON software (Blaauw and Christen, 2011). The model is based upon the radiocarbon dates of foraminifera given in Table 1. The small panels on top represent the Markov chain Monte Carlo iterations (a) and the distributions of the prior (green lines) and the posterior (gray histograms) for the accumulation rate (b) and memory (c). The bottom panel (d) illustrates the age–depth model. The blue dots depict the calibrated  $^{14}\text{C}$  ages. The gray stippled lines mark the 95 % confidence intervals. The red line reflects the single best model, based on the mean age for each depth. For more technical information, the reader is referred to Blaauw and Christen (2011).

progressively increase in two steps, culminating in a maximum at 10 ka (Fig. 3c). Afterwards, they decrease until the middle Holocene and increase again from 2 ka onwards. Concentrations of HMW *n*-alkanes show a similar development, but differences are evident. The concentrations of HMW *n*-alkanes share the two-step increase starting at 14.6 ka and subsequent decline, as well as the rise, during the late Holocene (Fig. 3b, c). However, while concentrations of HMW *n*-alkanoic acids are lowest during the early deglaciation (18–14.6 ka), the abundances of HMW *n*-alkanes are higher or similar to Holocene values (Fig. 3b). Between  $\sim 17.5$ –16.5 ka, concentrations of HMW *n*-alkanes are prominently elevated, reaching their maximum at that time. In contrast, HMW *n*-alkanoic acids reach maximum concentrations around 10 ka (Fig. 3b, c).

#### 4.2 Isotopic composition of HMW *n*-alkanoic acids

$\delta D_{\text{wax } n\text{-alkanoic acid}}$  range between  $-104\text{‰}$  and  $-153\text{‰}$ . The *n*-C<sub>26:0</sub> and *n*-C<sub>28:0</sub> alkanic acids behave similarly regarding  $\delta D$  values and trends (Fig. 4d; green and or-

ange lines). In general,  $\delta D_{\text{wax } n\text{-alkanoic acid}}$  is higher during the deglacial than during the Holocene (Fig. 4d). Two episodes of remarkable change are evident, i.e., between  $\sim 17.5$ –14.5 ka and between  $\sim 11$ –6 ka. At 17.5 ka,  $\delta D_{\text{wax } n\text{-alkanoic acid}}$  rapidly increase and reach maximal values at 17.0 ka. Afterwards, at  $\sim 16$  ka,  $\delta D_{\text{wax } n\text{-alkanoic acid}}$  decrease again, reaching values similar to the late Holocene. At 14.5 ka,  $\delta D_{\text{wax } n\text{-alkanoic acid}}$  slightly increase again and then remain relatively constant until a striking minimum is registered between 10.0–6.0 ka. The minimum begins and terminates abruptly (where abruptly is defined as being within a few hundred years). At this time, HMW *n*-alkanoic acids are depleted by 34‰, relative to the values found at 12 ka (Fig. 4d). After the minimum, there is little variability throughout the late Holocene.

Interestingly, comparing our  $\delta D_{\text{wax } n\text{-alkanoic acid}}$  with previously published  $\delta D_{\text{wax}}$  of HMW *n*-alkanes ( $\delta D_{\text{wax } n\text{-alkanes}}$ ) from the same core (Fig. 4d; blue line; Castañeda et al., 2016a) reveals distinct discrepancies. While  $\delta D_{\text{wax } n\text{-alkanoic acid}}$  and  $\delta D_{\text{wax } n\text{-alkanes}}$  from GeoB7702-3 are similar before 15 ka and at 1 ka, they differ in the long-term

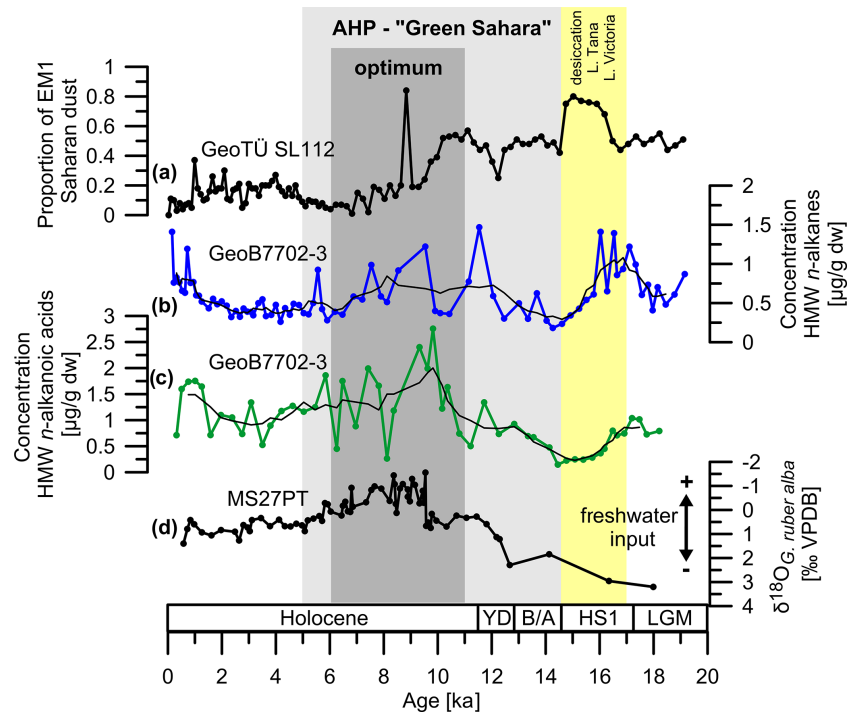


**Figure 3.** Concentrations of HMW *n*-alkanoic acids (even-numbered homologues  $\Sigma C_{26:0}$ – $C_{32:0}$ ; green; **c**) and HMW *n*-alkanes (odd-numbered homologues  $\Sigma C_{29}$ – $C_{33}$ ; blue; **b**) in core GeoB7702-3. Black lines denote running averages. **(a)** Endmember modeling results from the grain size analysis in core GeoTü SL112, adopted from Hamann et al. (2008). The contribution of endmember 1 (EM1) to the silt fraction represents Saharan dust input to the eastern Mediterranean (Hamann et al., 2008). **(d)** The oxygen isotopic composition of the planktic foraminifera species *Globigerinoides ruber alba* ( $\delta^{18}O_{G. ruber alba}$ ) from core MS27PT (Fig. 1c), Nile deep-sea fan (Revel et al., 2010, 2015), is given to reflect freshwater runoff in the Nile river. LGM is the Last Glacial Maximum; HS1 is the Heinrich stadial 1; B/A is the Bølling–Allerød interstadial; YD is the Younger Dryas stadial. The light gray and dark gray shadings mark the episodes of the AHP and the green Sahara, as well as their optimum. The yellow bar denotes the interval when lakes Tana and Victoria desiccated (Stager et al., 2011; Lamb et al., 2007; Marshall et al., 2011; Williams et al., 2006).

trend of the glacial-to-Holocene evolution. The amplitude of the long-term development in the  $\delta D_{wax\ n-alkanes}$  is larger than in the  $\delta D_{wax\ n-alkanoic\ acid}$ , which is why the  $\delta D_{wax\ n-alkanes}$  values are more negative than the  $\delta D_{wax\ n-alkanoic\ acid}$  values (up to 25‰; Fig. 4d). This difference in amplitude mainly stems from a progressive decrease in  $\delta D_{wax\ n-alkanes}$  from 15 ka onwards and from a progressive increase after  $\sim 5$  ka (Fig. 4d), which is not recorded by  $\delta D_{wax\ n-alkanoic\ acids}$ . In contrast to the  $\delta D_{wax\ n-alkanes}$ , the  $\delta D_{wax\ n-alkanoic\ acid}$  remain quite stable between 15–11 ka and after  $\sim 6$  ka (Fig. 4d). Both records agree with respect to the presence of a maximum at  $\sim 17$  ka and a minimum between 10–7 ka (Fig. 4d).

## 5 Discussion

$\delta D_{wax}$  is dependent on the  $\delta D$  of the source water taken up by the plant during biosynthesis and thus can be used as tracer for  $\delta D$  of precipitation (e.g., Sachse et al., 2012, and references therein; Tierney et al., 2017). The  $\delta D$  of the source water, in turn, varies, along with hydrological

processes including rainfall amount, evapotranspiration and moisture source, but temperature changes also affect the isotopic composition (Sachse et al., 2012). In low-latitude regions,  $\delta D_{wax}$  is predominantly influenced by rainfall amount (amount effect) as temperature effects are negligible (Sachse et al., 2012). This makes  $\delta D_{wax}$  a powerful tool to reconstruct glacial–interglacial fluctuations in rainfall amount and moisture source across Africa (Schefuß et al., 2005; Tierney et al., 2008; Berke et al., 2012; Costa et al., 2014; Collins et al., 2013; Castañeda et al., 2016a). As for the arid Sahara, Tierney et al. (2017) document that temperature effects play a subordinate role, while precipitation exerts predominant control on the  $\delta D_{wax}$ . However, changes in the relative abundance of  $C_3$  versus  $C_4$  plants may also overprint the hydrological signal in  $\delta D_{wax}$ , owing to different fractionation factors in the Calvin and Hatch–Slack photosynthetic pathways (e.g., Sachse et al., 2012; Collins et al., 2013). The stable carbon isotopic composition of leaf wax lipids ( $\delta^{13}C_{wax}$ ) is a common means to assess past changes in the relative contributions of  $C_3$  versus  $C_4$  plants in the catchment (Sachse et al., 2012; Collins et al., 2013) and to evaluate potential

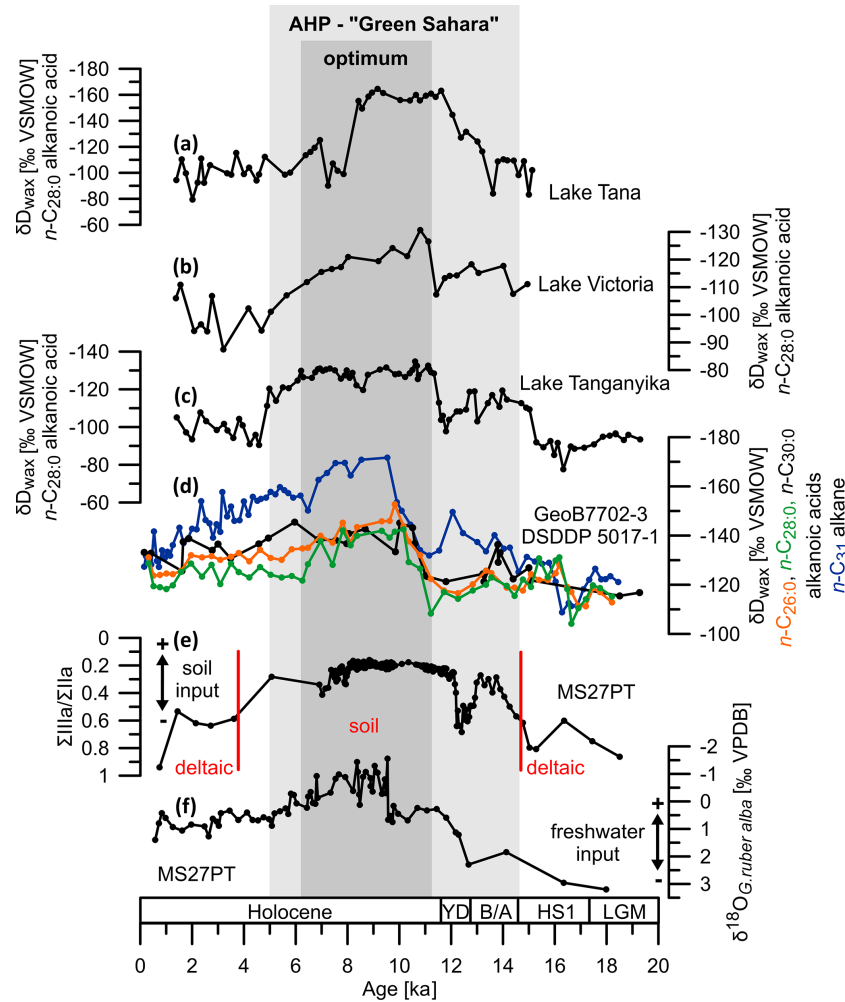


**Figure 4.** (a–c)  $\delta D_{\text{wax}}$  records from lakes Tana (Costa et al., 2014), Victoria (Berke et al., 2012) and Tanganyika (Tierney et al., 2008) reporting hydroclimate variability in tropical East Africa. (d)  $\delta D_{\text{wax}}$   $n$ -alkanoic acids (orange is  $n$ -C<sub>26:0</sub>; green is  $n$ -C<sub>28:0</sub>; this study), along with  $\delta D_{\text{wax}}$   $n$ -alkane (blue is  $n$ -C<sub>31</sub>; Castañeda et al., 2016a, b) from core GeoB7702-3 and  $\delta D_{\text{wax}}$ , based on the  $n$ -C<sub>30:0</sub> alkanolic acid from core DSDDP 5017-1 from the Dead Sea (black; Tierney et al., 2022). (e) Ratio of tetra- and pentamethylated brGDGTs from the Nile deep-sea fan (core MS27PT; Fig. 1) reporting on the input of delta-derived organic matter versus material from the soils in the upper Nile river catchment to the eastern Mediterranean (Ménot et al., 2020). (f) Oxygen isotopic composition of the planktic foraminifera species *Globigerinoides ruber alba* from the Levantine Basin (core MS27PT; Fig. 1) used to reconstruct changes in salinity related to Nile river runoff (Revel et al., 2010, 2015). The light gray and dark gray shadings mark the episodes of the AHP and the green Sahara and their optimum. LGM is the Last Glacial Maximum; HS1 is the Heinrich stadial 1; B/A is the Bølling–Allerød interstadial; YD is the Younger Dryas stadial.

impacts of vegetation changes on  $\delta D_{\text{wax}}$  (e.g., Castañeda et al., 2016a; Collins et al., 2013). To explore potential effects of vegetation changes on our  $\delta D_{\text{wax}}$   $n$ -alkanoic acid record, we correlate  $\delta D_{\text{wax}}$   $n$ -alkanoic acid and  $\delta^{13}\text{C}_{\text{wax}}$   $n$ -alkanoic acids (Fig. S1). Considering that the linear correlation yields low correlation coefficients ( $R^2 < 0.5$ ; Figs. S1 and S2), the impact of vegetation change on  $\delta D_{\text{wax}}$   $n$ -alkanoic acid is considered minor when the entire 18 kyr are considered. Nevertheless, considerable impacts from vegetation changes may have existed during shorter intervals, despite the weak correlation. The amplitudes in the  $\delta^{13}\text{C}_{\text{wax}}$   $n$ -alkanoic acids are rela-

tively small (up to 3‰), rendering profound impacts of vegetation changes on  $\delta D_{\text{wax}}$   $n$ -alkanoic acid unlikely. When correcting  $\delta D_{\text{wax}}$   $n$ -alkanoic acid for vegetation changes (see the Supplement), the patterns and amplitudes persist (Figs. S1, S3). We conclude that hydrologic variations exerted dominant control on  $\delta D_{\text{wax}}$   $n$ -alkanoic acid and that  $\delta D_{\text{wax}}$   $n$ -alkanoic acid is a robust proxy for changes in rainfall and moisture source in the Nile river watershed throughout the past 18 kyr.

To deduce deglacial changes in hydroclimate in the Nile river catchment, we pair our  $\delta D_{\text{wax}}$   $n$ -alkanoic acid with the  $\delta D_{\text{wax}}$   $n$ -alkanes from Castañeda et al. (2016a).  $\delta D_{\text{wax}}$   $n$ -alkanes

has been interpreted to reflect rainfall variability in the Nile river watershed associated with changes in the African summer monsoon (Castañeda et al., 2016a).

Similar  $\delta D_{\text{wax } n\text{-alkanoic acid}}$  and  $\delta D_{\text{wax } n\text{-alkanes}}$  before 15 ka and from 1 ka onwards (Fig. 4d) suggest that the compounds reflect the same signal at these times. Between 15–1 ka, the offset in  $\delta D_{\text{wax } n\text{-alkanoic acid}}$  and  $\delta D_{\text{wax } n\text{-alkanes}}$  (Fig. 4d) indicates that the compounds represent different hydrological developments, which in turn implies that HMW *n*-alkanoic acids and HMW *n*-alkanes derive from different source areas during this interval. This conclusion seems reasonable, considering that the Nile river watershed extends over several climate zones and covers strong hydrological contrasts (tropical to subtropical and hyperarid desert). These zones are influenced by different atmospheric circulation patterns, with the westerlies influencing the middle and lower catchments and the African monsoon controlling precipitation in the headwaters. Hence, the paired application of  $\delta D_{\text{wax } n\text{-alkanoic acid}}$  and  $\delta D_{\text{wax } n\text{-alkanes}}$  has the potential to reconstruct monsoonal, along with westerly, precipitation in the Nile river watershed. In the following, we evaluate from which section of the watershed HMW *n*-alkanoic acids and HMW *n*-alkanes derive to understand the hydrologic signals recorded in  $\delta D_{\text{wax } n\text{-alkanoic acid}}$  and  $\delta D_{\text{wax } n\text{-alkanes}}$ .

### 5.1 Source areas of leaf wax lipids in the Nile river watershed

Leaf wax lipids reach the ocean mainly via fluvial discharge but also through aeolian transport (Schlünz and Schneider, 2000; Kusch et al., 2010; Schreuder et al., 2018). The latter is most important in open-ocean settings, where river discharge has little influence (Kusch et al., 2010; Hedges et al., 1997). Off large river systems, leaf waxes are predominantly introduced by river discharge (e.g., Kusch et al., 2010), and accordingly, leaf waxes in the sediments of the Nile deep-sea fan (e.g., Blanchet et al., 2014) and at site GeoB7702-2 (Castañeda et al., 2016a) have been interpreted as recorders of environmental change in the Nile river watershed. However, in sediments of the southeastern Levantine Basin, the proportion of Saharan dust rises with increasing distance to the Nile delta (e.g., Krom et al., 1999). In core GeoB7702-3, concentrations of HMW *n*-alkanoic acids resemble the  $\delta^{18}\text{O}$  record of the planktonic foraminifera species *Globigerinoides ruber alba* ( $\delta^{18}\text{O}_{G. ruber alba}$ ; Fig. 3c, d) from a sediment core from the Nile deep-sea fan (MS27PT; Fig. 1) which tracks freshwater discharge from the Nile river (Revel et al., 2010). These records document that input of HMW *n*-alkanoic acids and river runoff were relatively low during the LGM and the early deglaciation and increased between 14–10 ka. During the middle Holocene, both declined (Fig. 3c, d). Similarly, HMW *n*-alkane concentrations point to rising input of terrigenous organic matter between 14–10 ka and a subsequent decline. This confirms that fluvial discharge was mainly responsible for the delivery of HMW *n*-alkanoic acids and

HMW *n*-alkanes to the eastern Mediterranean. However, the concentrations of HMW *n*-alkanes also have similarities with the proportion of Saharan dust in the sediments of the southeastern Levantine Basin (Hamann et al., 2008), in particular during the early deglaciation, before  $\sim 15$  ka (Fig. 3a, b). Both concentrations of HMW *n*-alkanes and the proportion of Saharan dust are relatively high compared to the AHP and late Holocene. Thus, dust-associated HMW *n*-alkanes may have additionally been deposited at site GeoB7702-3 at these times when fluvial discharge was low. Considerable Saharan dust contributions are documented until 10 ka (Hamann et al., 2008; Fig. 3a). Accordingly, aeolian transport may have been relevant to HMW *n*-alkanes at the study site from the last glacial until the early Holocene. Possible dust sources to the southeastern Levantine Basin are the eastern Libyan Desert, central Algeria, Egypt and Sudan (Hamann et al., 2008). Since dust input from the Sahara was relatively stable between 14.6–10 ka (Fig. 3a; Hamann et al., 2008), it is unlikely that variations in aeolian contributions from distal source regions outside the Nile river watershed account for the divergence in the  $\delta D_{\text{wax}}$  records. Thus, the offset in  $\delta D_{\text{wax}}$  in core GeoB7702-3 may be due to variations in source areas of HMW *n*-alkanoic acids and HMW *n*-alkanes within the Nile river watershed.

To identify the source areas of HMW *n*-alkanes and HMW *n*-alkanoic acids in GeoB7702-3 at present, we converted the  $\delta D_{\text{wax}}$  values into  $\delta D$  values of precipitation corrected for changes in vegetation and ice volume ( $\delta D_{\text{p-vc-ic}}$ ), according to the methods described in the Supplement.

We compare the near-core-top values (here 15 cm, translating to 0.31 kyr) to mean weighted  $\delta D$  values of precipitation of the growing season ( $\delta D_{\text{p-gs}}$ ) in the Nile catchment, using the data set by Bowen et al. (2005). Bowen et al. (2005) define the growing season as months with mean temperatures  $> 0^\circ\text{C}$ . According to this definition, the values reported for the Nile river watershed are monthly weighted annual means, since mean temperatures never drop below  $0^\circ\text{C}$  (<https://en.climate-data.org>, last access: 14 December 2022, AM Online Projects – Alexander Merkel, 2022a–e).  $\delta D_{\text{p-gs}}$  values from different parts of the catchment and the results from our  $\delta D_{\text{p-vc-ic}}$  are listed in Table 2. The  $\delta D_{\text{p-vc-ic}}$  results downcore are given in Fig. S3. For the core top,  $\delta D_{\text{p-vc-ic}}$  is around  $-14\text{‰}$  for the *n*-C<sub>31</sub> alkane and is  $-11\text{‰}$  and  $-8\text{‰}$  for the *n*-C<sub>26:0</sub> and *n*-C<sub>28:0</sub> alkanolic acids, respectively. This matches the isotopic composition of the Nile delta, where the predicted  $\delta D_{\text{p-gs}}$  range between  $-15$  and  $-11\text{‰}$  (at Cairo,  $30^\circ 3' \text{N}$ , and Alexandria,  $31^\circ 13' \text{N}$ ; Bowen et al., 2005). Today, the Nile river delta region receives the most deuterium-depleted precipitation in the entire watershed (Table 2; Bowen et al., 2005). In the middle section of the catchment, along the main Nile ( $30\text{--}15^\circ \text{N}$ ),  $\delta D_{\text{p-gs}}$  becomes progressively more enriched towards the south ( $-4\text{‰}$  at Aswan,  $24^\circ 6' \text{N}$ , and  $10\text{‰}$  in Khartoum,  $15^\circ 35' \text{N}$ ). In the headwater region, precipitation is more depleted compared to the main Nile but still is enriched by  $10\text{‰--}17\text{‰}$  ( $3.5\text{‰}$

Lake Tana, 12° N, and  $-5.6\%$  Lake Victoria, 1° S; Table 2) relative to  $\delta D_{p-gs}$  in the delta (Bowen et al., 2005). As such, we infer that HMW *n*-alkanoic acids and HMW *n*-alkanes predominantly derive from the delta region at present.

The offset between the  $\delta D_{wax\ n-alkanoic\ acid}$  and  $\delta D_{wax\ n-alkanes}$  between 15–1 ka (Figs. 4d, 5e) suggests that either the source of the HMW *n*-alkanoic acid or the HMW *n*-alkanes changed during this time frame. Considering that northeastern African hydroclimate saw drastic changes during the AHP (Shanahan et al., 2015; Berke et al., 2012; Tierney et al., 2008; Costa et al., 2014), it is very likely that the gradients in  $\delta D_{p-gs}$  changed too. Accordingly, the present-day distribution of  $\delta D_{p-gs}$  cannot be used for paleo source apportionment. Unfortunately, the detailed spatial distribution of past  $\delta D_{p-gs}$  in the Nile river watershed remains unresolved, preventing us from using our  $\delta D_{p-vc-ic}$  to identify the source areas of the leaf waxes during the last glacial and the deglaciation. Therefore, we compare our  $\delta D_{wax}$  records to the available  $\delta D_{wax}$  data from lakes Tana, Victoria and Tanganyika (Figs. 1 and 3a–d) and to a  $\delta D_{wax}$  record from the Dead Sea, representing hydroclimate variability in the headwaters, equatorial Africa and the eastern Mediterranean realm (Fig. 3a–d; Berke et al., 2012; Costa et al., 2014; Tierney et al., 2008, 2022).

Our  $\delta D_{wax\ n-alkanoic\ acid}$  has a remarkable resemblance with the  $\delta D_{wax}$  record from the Dead Sea (Tierney et al., 2022; Figs. 1, 4d). When plotted on the same scale, the two records track each other, sharing trends and amplitudes (Fig. 4d). Even the range of values covered by the two records is almost the same, varying between ca.  $-105\%$  to  $-145\%$  during the past 18 ka. These similarities suggest that the  $\delta D_{wax\ n-alkanoic\ acid}$  in core GeoB7702-3 was determined by Mediterranean hydroclimate throughout the past 18 ka. This also implies that the HMW *n*-alkanoic acids were constantly sourced from the lower Nile river catchment. Due to the larger amplitude in the long-term development of the  $\delta D_{wax\ n-alkanes}$ , the range of values covered ( $-105\%$  to  $-170\%$ ) is larger than in the  $\delta D_{wax\ n-alkanoic\ acid}$ . If the Dead Sea  $\delta D_{wax}$  and our  $\delta D_{wax\ n-alkanoic\ acid}$  reflect the composition of the Mediterranean moisture (Tierney et al., 2022), then the  $\delta D_{wax\ n-alkanes}$  must have been influenced by more depleted rainfall and thus by another moisture source. At Lake Tana,  $\delta D_{wax}$  values of up to  $-160\%$  have been recorded during the AHP (Costa et al., 2014), providing evidence that in the headwaters of the Blue Nile the rainfall was more depleted during the AHP than the Mediterranean precipitation (Fig. 4a). It is most likely that the HMW *n*-alkanes recorded climate variability in the southern reaches of the river, where the summer monsoon determines the hydroclimate. In equatorial Africa, decreasing  $\delta D_{wax}$  in sediments from Lake Tanganyika (Tierney et al., 2008) point to increasing humidity from 15 to 11.5 ka (Fig. 4c). Likewise, the levels from lakes Tana and Victoria – which desiccated during the late glacial (Stager et al., 2011; Lamb et al., 2007) – rose at that time in response to a wetter climate (Williams

et al., 2006; Marshall et al., 2011). Also,  $\delta D_{wax}$  of lakes Tana and Victoria document an increase in rainfall amount during the AHP (Costa et al., 2014; Berke et al., 2012; Fig. 4a, b). The progressive decrease in  $\delta D_{wax\ n-alkanes}$  starting at 15 ka thus is in harmony with the hydroclimate development in the headwaters during the early AHP, further corroborating our inference that the  $\delta D_{wax\ n-alkanes}$  was substantially influenced by rainfall in the southern Nile river catchment.

Accordingly, we propose that while the HMW *n*-alkanoic acids were constantly sourced from the delta region throughout the past 18 ka, the HMW *n*-alkanes in core GeoB7702-3 received considerable contributions from the headwater region between  $\sim 15$ –1 ka. Before and afterwards, both compounds were predominantly sourced from the delta. However, acknowledging that the Sahara was vegetated between  $\sim 11$ –5 ka (Kuper and Kröpelin, 2006; Watrin et al., 2009; Hély et al., 2014; Hamdan et al., 2016), the source region of the HMW *n*-alkanoic acids may have extended further south into the northern Sahara at this time. Likewise, the HMW *n*-alkanes probably received additional material from the middle catchment of the river. During the AHP, site GeoB7702-3 may also have received additional load from the Sinai Peninsula through Wadi El-Arish. This drainage basin is rather dry at present but activated during the AHP (AbuBakr et al., 2013; Muhs et al., 2013).

Our scenario regarding dynamics in HMW *n*-alkane provenance fits to findings from Ménot et al. (2020), who analyzed branched glycerol dialkyl glycerol tetraethers (brGDGTs) in the Nile deep-sea fan to reconstruct soil input from the Nile river into the eastern Mediterranean over the deglaciation. The brGDGTs are synthesized by bacteria thriving in peat and soils (Weijers et al., 2006; Martin et al., 2019) but can also be produced in situ in rivers and estuarine settings and in the marine sediments (De Jonge et al., 2014). Using the ratio between tetra- and pentamethylated brGDGTs ( $\Sigma IIIa / \Sigma IIa$ -ratio), Ménot et al. (2020) inferred that the compounds derived from the Nile delta between 20–14.5 ka and after 4 ka (Fig. 4e). The interval of soil-derived input (14.5–4 ka; Ménot et al., 2020) matches the interval of diverging  $\delta D_{wax\ n-alkanoic\ acid}$  and  $\delta D_{wax\ n-alkanes}$  (Fig. 4d) when considerable amounts of HMW *n*-alkanes from the upper and middle catchment were deposited in the eastern Mediterranean sediments.

Being hydrophobic, the HMW *n*-alkanes and HMW *n*-alkanoic acids are among the recalcitrant fraction of organic matter that is preserved for long times in the geological record and consequently is able to survive riverine transport and intermediate storage in reservoirs prior to burial in the marine sediments (e.g., Eglinton and Eglinton, 2008). However, our north–south allocation regarding the sources of HMW *n*-alkanoic acids and HMW *n*-alkanes in GeoB7702-3 suggests that in the Nile river watershed, most of the HMW *n*-alkanoic acids are sourced from the upper catchment and did not reach site GeoB7702-3, most likely due to degradation during riverine transport.

**Table 2.** Results for  $\delta D_{p\text{-vc-ic}}$  calculated based on  $\delta D_{wax}$  for GeoB7702-3 at 15 cm depth ( $\sim 0.3$  ka), together with  $\delta D_{p\text{-gs}}$  values across the Nile river watershed. Locations listed are indicated in Fig. 1.

Location	$\delta D_{p\text{-vc-ic}}$ (‰)	$\delta D_{p\text{-gs}}^1$ (‰)
GeoB7702-3; 15 cm; C <sub>31</sub> <i>n</i> -alkane	$-14.87 \pm 4.95$	
GeoB7702-3; 15 cm; C <sub>26:0</sub> <i>n</i> -alkanoic acid	$-11.10 \pm 3.14$	
GeoB7702-3; 15 cm; C <sub>28:0</sub> <i>n</i> -alkanoic acid	$-8.78 \pm 2.51$	
Cairo, Nile delta		-14.6 to -11.4
Alexandria, Nile delta		-13.1
Aswan, main Nile		-4.4
Dunqulā, main Nile		4.5 to 5.3
Khartoum, main Nile		9.9
Kassala, Atbara		13.4 to 9.7
Bahir Dar, Lake Tana		3.5
Juba, White Nile		5.9
Kampala, Lake Victoria		-5.6

<sup>1</sup> Adopted from Bowen et al. (2005).

Leaf-wax-based records from off-river mouths often are interpreted as catchment integrating signals (e.g., Blanchet et al., 2014; Häggi et al., 2016; Hemingway et al., 2016), as also done by Castañeda et al. (2016a) with respect to  $\delta D_{wax}$  *n*-alkanes in core GeoB7702-3. However, our results underscore previous studies, which indicate that this does not generally hold true for all types of lipids or for all river systems (Hemingway et al., 2016; Agrawal et al., 2014; Galy et al., 2011). It has been reported that leaf wax lipids may be representative for specific parts of a river catchment only, and source regions may vary between compound classes and even between homologues within a compound class (e.g., Hemingway et al., 2016; Agrawal et al., 2014). Hemingway et al. (2016) found that HMW *n*-alkanoic acids originate from a local source in the Congo River watershed, while HMW *n*-alkanes serve as catchment-wide integrator. Similarly, Agrawal et al. (2014) suggested that in the Ganga–Brahmaputra River system HMW *n*-alkanoic acids from the Himalayan headwaters degrade during transport and get replaced by HMW *n*-alkanoic acids from the local floodplains. Our inference that HMW *n*-alkanes are catchment integrators, while HMW *n*-alkanoic acids contain local signals from the lower river catchment, matches those previous findings. There is consensus that HMW *n*-alkanoic acids are more prone towards degradation than HMW *n*-alkanes (Meyers and Ishiwatari, 1993; Hoefs et al., 2002; Sinningh-Damsté et al., 2002; Galy and Eglinton, 2011; Hemingway et al., 2016), which probably accounts for the discrepancies in provenance of HMW *n*-alkanoic acids and HMW *n*-alkanes observed in these large river systems (e.g., Hemingway et al., 2016) and at our study site.

## 5.2 Environmental drivers of HMW *n*-alkane provenance

There is compelling evidence that during the LGM and the early deglaciation, in particular Heinrich stadial 1 (HS1), the

northeastern African climate was very arid (Stager et al., 2011; Castañeda et al., 2016; Tierney et al., 2008; Tierney and deMenocal, 2013; Revel et al., 2014; Ménot et al., 2020). Lakes Tana and Victoria, the sources of the Blue and White Nile tributaries, desiccated at 17–16 ka (Stager et al., 2011; Lamb et al., 2007), leading to a drastic reduction in runoff in the Nile river system relative to the present (Williams et al., 2009, 2015), as documented by higher  $\delta^{18}O_{G. ruber alba}$  (Figs. 3d, 4f) offshore the Nile river mouth (Revel et al., 2010, 2015). At the same time, the deposition of Saharan dust peaked in the eastern Mediterranean (Fig. 3a; Hamann et al., 2008). The weak fluvial activity in the Nile river likely restricted the source of the leaf wax lipids to the Nile delta and led to minimal export of HMW *n*-alkanoic acids in eastern Mediterranean sediments (Fig. 3c). Relatively high concentrations of HMW *n*-alkanes in core GeoB7702-3 despite the diminished fluvial activity (Fig. 3b) can be best explained by aeolian transport of HMW *n*-alkanes sourced from the vegetated Nile delta region and floodplain deposits of the lower Nile river catchment, considering that the input of Saharan dust to the eastern Mediterranean peaked at these times (Hamann et al., 2008; Fig. 3a).  $\delta D_{wax}$  records from Lake Tanganyika (Fig. 4c) document that the East African climate became wetter around 14.5–15 ka (Tierney et al., 2008). In response to the wetter conditions, the overflow of lakes Tana and Victoria resumed at around 15.5 and 14.5 ka (Williams et al., 2006; Marshall et al., 2011), and freshwater input from the Nile river increased accordingly, as documented by lower  $\delta^{18}O_{G. ruber alba}$  values (Fig. 4f; Revel et al., 2010, 2014, 2015). The climate amelioration in northeastern Africa coincides with the onset of divergence between  $\delta D_{wax}$  *n*-alkanes and  $\delta D_{wax}$  *n*-alkanoic acid, as well as with the switch from deltaic to soil-derived brGDGTs (Fig. 4d, e). Concentrations of HMW *n*-alkanes increase, along with decreasing  $\delta^{18}O_{G. ruber alba}$  (Fig. 3c, d), suggesting that enhanced fluvial energy in the headwaters probably increased

erosion and export of organic matter in the upper reaches of the river, as well as in the middle catchment, where vegetation expanded into the Sahara in the course of the AHP. Increasing concentrations of HMW *n*-alkanoic acids (Fig. 3c) likely reflect intensified fluvial erosion in the delta and floodplains of the lower Nile catchment. During the late Holocene, at around 5–4 ka, drier conditions re-established in the headwaters and tropical eastern Africa (Tierney et al., 2008; Costa et al., 2014; Berke et al., 2012), and Nile runoff reduced accordingly (Revel et al., 2010, 2015). Again, the delta became the predominant source of HMW *n*-alkanes and brGDGTs.

### 5.3 Hydroclimate development during the past 20 ka

For the reconstruction of the hydroclimate variability, our findings imply that the  $\delta D_{\text{wax } n\text{-alkanoic acid}}$  value documents Mediterranean winter rainfall throughout the past 18 ka, while  $\delta D_{\text{wax } n\text{-alkanes}}$  value should predominantly be a summer monsoon signal between  $\sim 14.5$ –4 ka.

### 5.4 LGM and Heinrich stadial 1 (18–14.6 ka)

Paleoenvironmental reconstructions suggest that the LGM ( $\sim 21$  ka; Clark et al., 2009) was a relatively moist interval in the southeastern Mediterranean realm, due to a more positive water balance (precipitation–evaporation) compared to today, as indicated by higher levels of glacial Lake Lisan (paleo Dead Sea; Fig. 1; Stein, 2001) and pollen data from Dead Sea sediments (Langgut et al., 2021). In the northeastern Sahara, tufa deposits from the eastern Desert provide evidence for sufficiently moist conditions to recharge aquifers (Hamdan and Brook, 2015). It is assumed that cold glacial conditions likely resulted in reduced evaporation and higher effective moisture during the LGM (Ludwig and Hochmann, 2021; Stockhecke et al., 2016). Moreover, stronger westerly winds over the North Atlantic and the Mediterranean region (Wang et al., 2008; Löfverström and Lora, 2017; Kageyama et al., 2021) likely enhanced the advection of moist air from the Atlantic Ocean and Mediterranean Sea to the southeastern Mediterranean borderlands, accounting for increased rainfall (Hamdan and Brook, 2015; Wang et al., 2018; Goldsmith et al., 2017; Enzel et al., 2008).

The northeastern African climate became harsher during the early deglaciation (from 19 ka onwards), with the most severe aridity occurring during HS1 ( $\sim 18$ –14.5 ka; Tierney et al., 2008; Stager et al., 2008; Hamdan and Brook, 2015). Lakes Victoria and Tana desiccated (Stager et al., 2011; Lamb et al., 2007), and in the eastern Sahara, tufa formation ceased (Hamdan and Brook, 2015). Also, in the Nile river delta, conditions may have rapidly become more arid at the beginning of HS1, given the abrupt increase in  $\delta D_{\text{wax } n\text{-alkanoic acid}}$  and  $\delta D_{\text{wax } n\text{-alkanes}}$  (Castañeda et al., 2016a) at  $\sim 17.8$  ka (Figs. 4d, 5e). Maximal values of  $\delta D_{\text{wax } n\text{-alkanoic acid}}$  and  $\delta D_{\text{wax } n\text{-alkanes}}$  also suggest that the Nile river delta had experienced the most arid condi-

tions since the LGM at that time. However, the drought was restricted to the first half of HS1. At  $\sim 16$  ka, the climate rapidly transitioned into a wet phase that lasted until the end of HS1 (14.6 ka) (Figs. 4d, 5e).  $\delta D_{\text{wax } n\text{-alkanoic acid}}$  values suggest that hydroclimatic conditions were as moist during the late Holocene, considering the similar values in  $\delta D$  ( $-130\text{‰}$  to  $-125\text{‰}$ ).

Tierney et al. (2022) documented that the glacial–interglacial hydroclimate of the Levant is quite sensitive to temperature-driven changes in the atmospheric evaporative demand. Warming enhances evapotranspiration and reduces effective moisture. The dry episode coincided with a moderate temperature rise, and the wet period occurred along with a cold phase in the eastern Mediterranean, as documented by TEX<sub>86</sub>-based temperature reconstructions from core GeoB7702-3 (Castañeda et al., 2010a; Fig. 5f). Early warming may have reduced moisture availability in the region by enhancing evapotranspiration. Later, the reversal to colder conditions may have weakened evapotranspiration, allowing for more effective moisture.

Next to temperature-induced changes in evaporation, variations in rainfall amount due to altered atmospheric circulation patterns are potential drivers that need to be evaluated. Wetter conditions in the southeastern Mediterranean are associated with enhanced cyclonic activity (Cyprus lows) over the eastern Mediterranean (Alpert et al., 1990). However, as noted by Bartov et al. (2003), lower air temperatures that possibly came along with low sea surface temperatures (SSTs) in the eastern Mediterranean during HS1 (Bar-Matthews et al., 1999) would have minimized the intensity and frequency of Cyprus lows, which would have reduced the advection of moist air and rainfall to the southeastern Mediterranean realm and fostered aridity. This is at odds with the isotopic depletion of the leaf waxes documented in core GeoB7702-3. If the local cyclonic activity and rainfall were weakened, either the effects of less evaporation must have balanced the reduced advection of moisture from the Cyprus lows, or another moisture source must have provided the Nile river delta region with rainfall. Interestingly, Italian speleothems imply that the delivery of Atlantic moisture to the central Mediterranean intensified from  $\sim 16$  ka onwards (Columbu et al., 2022). Analogous to the Italian site, a stronger influence of the Atlantic moisture may have caused more humid conditions in the Nile river delta.

The succession of dry and wet episodes within HS1 recorded at our study site fits the growing view that HS1 evolved in two phases, with the first lasting from  $\sim 18.2$ –16.2 ka and the second lasting from 16.2–14.5 ka (e.g., Naughton et al., 2023, and references within). Two-phase patterns with alternating dry and wet intervals have also been recorded by many marine and terrestrial archives in the entire Mediterranean realm (Valsecchi et al., 2012; Naughton et al., 2023; Naughton et al., 2009, 2016; Pérez-Mejías et al., 2021; Fletcher and Sanchez-Goñi et al., 2008) and even in western North America, where they have been

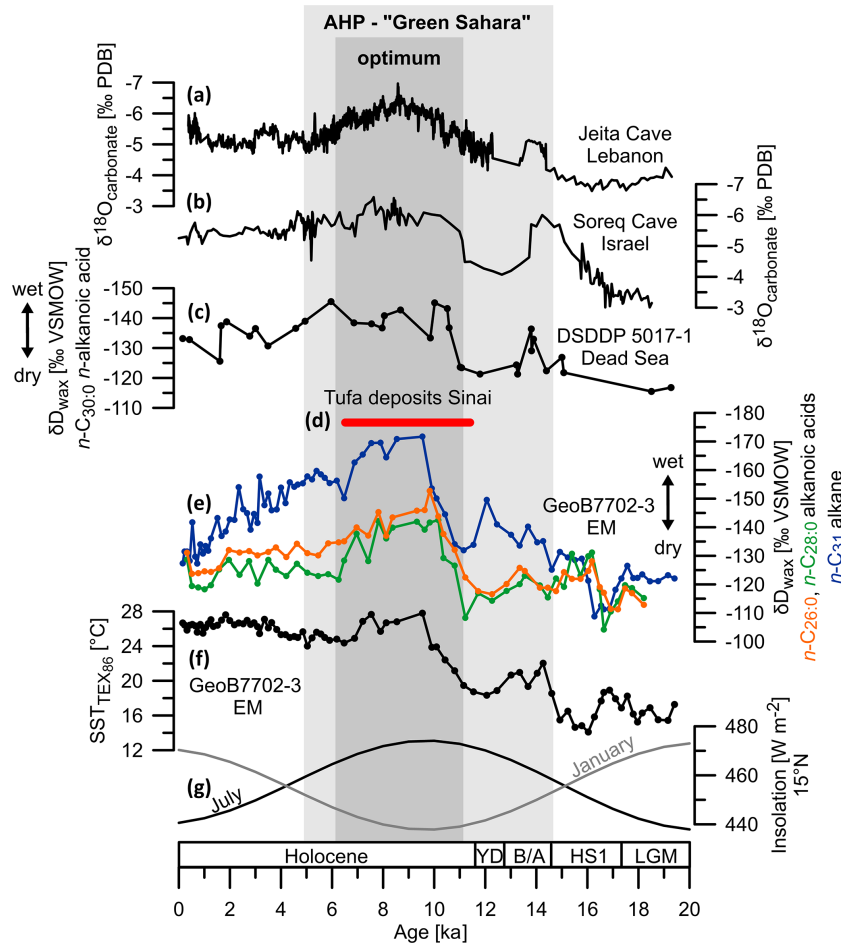


**Figure 5.** (a) Oxygen isotope records from speleothems ( $\delta^{18}\text{O}_{\text{carbonate}}$ ) in Jeita Grotto, Lebanon (Cheng et al., 2015). (b) Oxygen isotope records from speleothems in Soreq Cave, Israel (Bar-Matthews et al., 2003). (c)  $\delta\text{D}_{\text{wax}}$  record, based on the  $n\text{-C}_{30:0}$  alkanic acid in core DSDDP 5017-1 from the Dead Sea (Fig. 1; Tierney et al., 2022). (d) The red bar marks the interval during which spring tufa deposits formed on the Sinai Peninsula (Hamdan and Brook, 2015). (e)  $\delta\text{D}_{\text{wax}}$   $n$ -alkanoic acids (orange is  $n\text{-C}_{26:0}$ ; green is  $n\text{-C}_{28:0}$ ; this study), along with  $\delta\text{D}_{\text{wax}}$   $n$ -alkane (dark green is  $n\text{-C}_{31}$ ; Castañeda et al., 2016a, b), from core GeoB7702-3. (f) Sea surface temperature (SST) in the eastern Mediterranean (EM), based on  $\text{TEX}_{86}$  from core GeoB7702-3 (Castañeda et al., 2010a, c). (g) Insolation during January and July at  $15^\circ\text{N}$  from Berger and Loutre (1991). The light gray and dark gray shadings indicate the episodes of the AHP and the green Sahara and their optimum. LGM is the Last Glacial Maximum; HS1 is the Heinrich stadial 1; B/A is the Bølling–Allerød interstadial; YD is the Younger Dryas stadial.

called “big dry” and “big wet” intervals (Broecker et al., 2009). However, the Mediterranean records are inconsistent regarding the order of wet and dry episodes. For example, the Sea of Marmara (northeastern Mediterranean) experienced wet conditions during the first phase of HS1, followed by drought during the second phase (Valsecchi et al., 2012). The opposite pattern is evident in our data at site GeoB7702-3. As elaborated by Naughton et al. (2023) and references therein, these inconsistencies indicate a complex hydroclimate development in the Mediterranean borderlands throughout HS1.

At the end of HS1, relatively dry conditions established in the Nile river delta region and prevailed until 11.5 ka, as documented by increased  $\delta\text{D}_{\text{wax}}$   $n$ -alkanoic acid (Fig. 5e). The storm frequency and westerly moisture supply probably re-

mained relatively weak in the region throughout this period. Warming after HS1 (Fig. 5f) may have intensified evapotranspiration fostering aridity in the region.

### 5.5 African humid period (14.5–5 ka)

Whereas  $\delta\text{D}_{\text{wax}}$   $n$ -alkanoic acid indicate relatively constant dryness after HS1,  $\delta\text{D}_{\text{wax}}$   $n$ -alkanes document a progressive depletion of plant waxes. As previously discussed by Castañeda et al. (2016a), this progressive depletion starting at  $\sim 15$  ka most likely stems from increasing rainfall amount in the headwaters of the Nile river catchment. This development agrees with increasing humid conditions at lakes Tanganyika, Tana and Victoria and has been interpreted as the intensifica-

tion of the African summer monsoon (Castañeda et al., 2016; Berke et al., 2012; Tierney et al., 2008; Costa et al., 2014). This hydroclimate amelioration led into in the AHP which lasted from  $\sim 14.5$ – $5$  ka and culminated between  $\sim 11$ – $6$  ka (e.g., deMenocal et al., 2006a; Tierney et al., 2017; Dupont and Schefuß, 2018). More negative  $\delta D_{\text{wax } n\text{-alkanoic acid}}$  values also indicate that the Nile river delta received substantially more rainfall during the AHP optimum, i.e., between 11.0–6.0 ka (Fig. 5e).

A case study conducted by Breitenbach et al. (2010) in the Bay of Bengal/Indian Ocean shows that intensified river discharge due to heavy summer monsoon rainfall leads to surface water freshening in the Ocean, which in turn lowers the  $\delta D$ -signature of precipitation derived from these surface waters. Likewise, the discharge of isotopically light water from the Nile river watershed varied along with monsoon intensity during the Late Quaternary (Almogi-Labin et al., 2009). Isotopic variations in the Mediterranean surface waters may explain parts of the  $\delta^{18}\text{O}$  signals recorded in speleothems from caves in Israel and Lebanon (Cheng et al., 2012) and  $\delta D_{\text{wax}}$  from the Dead Sea (Tierney et al., 2022). Considering that the  $\delta^{18}\text{O}_{G. ruber alba}$  records from the Mediterranean Sea (Emeis et al., 2000; Revel et al., 2010, 2015) show massive surface freshening during the AHP resulting from enhanced monsoon rains in the Nile river watershed, this effect could have potentially accounted for depleted  $\delta D_{\text{wax } n\text{-alkanoic acid}}$  in addition to or instead of the amount effect. However, given that the  $\delta^{18}\text{O}_{G. ruber alba}$  (Revel et al., 2010, 2015) and  $\delta D_{\text{wax } n\text{-alkanoic acid}}$  show different temporal trends (Fig. 4d, f), freshening of the Mediterranean probably constitutes only a minor part of the signal in  $\delta D_{\text{wax } n\text{-alkanoic acid}}$ . Therefore, the minimum in  $\delta D_{\text{wax } n\text{-alkanoic acid}}$  most likely attests to the drastically increased amount of effective moisture in the Nile river delta during the AHP.

TEX<sub>86</sub>-based SST reconstructions at site GeoB7702-3 show pronounced warming at 11–10 ka (Fig. 5f; Castañeda et al., 2010a). As warming enhances evapotranspiration and reduces effective moisture, a more negative water balance due to elevated evapotranspiration would be expected. However, an increase in evapotranspiration and reduction in effective moisture would cause an isotopic enrichment of the leaf waxes rather than a depletion (Sachse et al., 2012). As such, the decrease in  $\delta D_{\text{wax } n\text{-alkanoic acid}}$  reported at site GeoB7702-3 clearly documents that increased rainfall must have exceeded any potential increases in evaporation, thereby leading to a more positive water balance.

It is well constrained that the ITCZ and summer monsoon shifted northward during the AHP, supplying the Sahara with seasonal rainfall (e.g., deMenocal et al., 2006b; Menviel et al., 2021; Braconnot et al., 2007; Blanchet et al., 2021; Tierney et al., 2017; Kuper and Kröpelin, 2006; Hamdan and Brook, 2015). The northernmost extent of the summer monsoon is still a matter of debate, in particular for the northwestern Sahara (Pausata et al., 2016; Thompson et al., 2019, 2021; Chandan and Peltier, 2020; Tierney et al., 2017;

Cheddadi et al., 2021). As for the northeastern Sahara, several proxy data and climate models collectively suggest that the monsoon fringe did not reach the Nile delta region during the AHP. Climate models operating with vegetation and dust feedbacks set the limit of the monsoon between 22–25° N (Pausata et al., 2016, Dallmeyer et al., 2020; Thomsson et al., 2019). This view is consistent with dust accumulation rates in the Red Sea, which indicate the northernmost extent of monsoonal rains at 22° N over northeastern Africa (Palchan and Torfstein, 2019). Further support comes from Holocene spring tufa deposits in the Eastern Desert and the Sinai Peninsula (Hamdan and Brook, 2015). The tufas from the Eastern Desert ( $\sim 25^\circ$  N) were fed from monsoonal precipitation, whereas tufa from the Sinai Peninsula (at  $\sim 27^\circ$  N) precipitated from springs recharged by Mediterranean rainfall (Hamdan and Brook, 2015). Moreover, salinity reconstructions from the Red Sea (Arz et al., 2003) suggest that the Mediterranean was the predominant moisture source to the northeasternmost region of Africa during the Holocene. Thus, instead of monsoonal rain, increased winter precipitation associated with the westerlies was most likely responsible for the enhanced rainfall in the Nile delta between 11–6.5 ka.

### 5.5.1 Controls on enhanced winter precipitation

The rapid switch to wetter conditions at 11 ka, as well as the abrupt return to dry conditions at 6.5 ka displayed by the  $\delta D_{\text{wax } n\text{-alkanoic acid}}$ , occurred congruently with a warm phase in the eastern Mediterranean, as documented by the TEX<sub>86</sub>-temperature proxy from GeoB7702-3 (Fig. 5e, f; Castañeda et al., 2010a). The warm SST enhanced evaporation over the Mediterranean Sea and at the same time led to a higher water-holding capacity of the atmosphere in virtue of the Clausius–Clapeyron relation (e.g., Trenberth et al., 2003; Lenderink and Meijgaard, 2008). Additionally, warming may have strengthened the formation of Cyprus lows over the Levantine Basin. Both effects would have increased moisture delivery to the Nile river delta region. Records from the Middle East (e.g., Jeita Grotto and Soreq Cave and Dead Sea; Fig. 5a, b, c), southern Europe and northwestern Africa provide evidence that mild and wet conditions were widespread across the Mediterranean borderlands during the early Holocene (Cheddadi et al., 2021; Wagner et al., 2019; Bar-Matthews et al., 2003; Cheng et al., 2015; Tierney et al., 2022). Today, relatively mild and wet winters in the southern Mediterranean realm are associated with negative phases of the NAO index, during which the westerlies weaken and the Atlantic storm track is situated south steering Atlantic moisture and storms frequently into the Mediterranean (Fig. 1). As invoked by several data, as well as model-based studies, negative NAO-like circulation patterns probably prevailed during the early Holocene, promoting intense winter precipitation in the Mediterranean borderlands (Kutzbach et al., 2014; Arz et al., 2003; Dixit et al.,

2020; Wassenburg et al., 2016). Previous work suggests that the southward displacement of the westerlies and the associated storm trajectory was a response to decreasing Northern Hemisphere winter insolation and thus a result of precessional forcing (Kutzbach et al., 2014; Wagner et al., 2019; Li et al., 2019). Analyzing lacustrine sediments from Lake Ohrid (Balkan Peninsula), Wagner et al. (2019) proposed that the Mediterranean winter precipitation varied in-phase with the African summer monsoon strength over glacial–interglacial cycles, as both were driven by precessional and thus insolation forcing. The monsoon responded to rising summer insolation changes and Mediterranean precipitation to weakened winter insolation (Wagner et al., 2019; Cheng et al., 2016). Indeed,  $\delta D_{\text{wax } n\text{-alkanoic acid}}$  and  $\delta D_{\text{wax } n\text{-alkanes}}$  from core GeoB7702-3 confirm that Mediterranean winter rains and the African summer monsoon (Castañeda et al., 2016a; Costa et al., 2014; Berke et al., 2012; Tierney et al., 2008) were concurrently strong in the Nile river watershed during the AHP optimum, but wet conditions began later ( $\sim 11$  ka) in the delta than in the upper river catchment ( $\sim 14.5$  ka; Figs. 4a–d, 5e). The relatively short wet phase recorded in our  $\delta D_{\text{wax } n\text{-alkanoic acid}}$  agrees with the timing of pronounced freshening of the northern Red Sea which has been interpreted to result from enhanced winter rainfall over Egypt and the Sinai Peninsula (Arz et al., 2003). Moreover, spring tufa deposits formed on the Sinai Peninsula only between 9.0–6.7 ka (Fig. 5d) and were fed by Mediterranean moisture (Hamdan and Brook, 2015). Together, these data show that in the northeastern Sahara wet conditions were restricted to the AHP optimum (11.0–6.5 ka).

### 5.5.2 Implications for the green Sahara (11–5 ka)

Providing insights into the development of summer and winter precipitation in the Nile river watershed, our findings are important for the understanding of the moisture sources which sustained the green Sahara. It is widely accepted that the northward migration and intensification of the summer monsoon was critical to trigger plant growth in the Sahara during the AHP (Braconnot et al., 2007; Menviel et al., 2021; deMenocal et al., 2000b; Shanahan et al., 2015; Sha et al., 2019; Tierney et al., 2017). However, discrepancies between proxy data and climate simulations regarding precipitation and vegetation anomalies (Chandan et al., 2020; Braconnot et al., 2007; Hopcroft et al., 2017; Perez-Sanz et al., 2014; Cheddadi et al., 2021; Hély et al., 2014; Tierney et al., 2017) raise the question of whether the monsoon was the only moisture source to sustain a green Sahara between 25–31° N (Cheddadi et al., 2021; Thompson et al., 2019, 2021). According to vegetation reconstructions, savannah was centered between 20–25° N, partly reaching  $\sim 28$ –31° N (Larrasoña et al., 2013; Hély et al., 2014; Giraudi et al., 2013; Hamdan et al., 2016). The northeastern Sahara, south of the Nile delta, turned into a semi-arid landscape covered by patchy vegetation comprising desert and open-

grass savannah, as well as Mediterranean vegetation near the coast (Hamdan et al., 2016; Larrasoña et al., 2013). Wetlands and trees likely flourished near permanent waterbodies such as the Faiyum Oasis (Hamdan et al., 2016; Watrin et al., 2009). Thus, since the monsoon extended no further than  $\sim 22$ –25° N over northeastern Africa (e.g., Palchan and Torfstein, 2019; Arz et al., 2003), it likely was insufficient to support such vegetation in the lower Nile river basin.

Our  $\delta D_{\text{wax } n\text{-alkanoic acid}}$  show that Mediterranean winter rainfall enhanced during the AHP optimum and most likely created favorable conditions for the establishment of the desert steppe vegetation around the Nile delta at these times. The modern winter rainfall zone is restricted to a small area along the Mediterranean coast (between  $\sim 30$ –31° N over northeastern Africa). If winter rains not only intensified but also protruded deeper into the Sahara, they may have provided the moisture needed to sustain the grasslands north of 22° N in the northeastern Sahara (Cheddadi et al., 2021; Larrasoña et al., 2013; Hamdan et al., 2016).

Seeking evidence that the winter rainfall zone extended deeper into the Sahara, the information could potentially be in the  $\delta D_{\text{wax } n\text{-alkane}}$ , considering that HMW *n*-alkanes received substantial contributions from the upper and middle catchment during the AHP. At  $\sim 11$  ka – at the onset of the AHP and green Sahara optimum – the  $\delta D_{\text{wax } n\text{-alkane}}$  shows a reversal to enriched  $\delta D$  values (Fig. 5e). The reversal may either be interpreted as a reduction in rainfall amount or as a change in the moisture source. Castañeda et al. (2016a) suggested the reversal would attest to drier conditions during the Younger Dryas stadial. However, our revised age model for GeoB7702-3 (Table 1) suggests that the reversal most likely occurred after the Younger Dryas (Fig. 5e).

A similar reversal is not present in the  $\delta D_{\text{wax}}$  records from lakes Tana and Victoria (Fig. 4a, b; Berke et al., 2012; Costa et al., 2014). These records even suggest that the monsoonal rainfall reached its maximum in the headwaters at this time (Fig. 4a, b). Therefore, it is unlikely that the reversal in  $\delta D_{\text{wax } n\text{-alkane}}$  stems from a weakened monsoon. A comparable signal is also missing in  $\delta D_{\text{wax } n\text{-alkanoic acid}}$  and the  $\delta D_{\text{wax}}$  record from the Dead Sea (Fig. 4d). We conclude that the signal most likely was generated in the middle part of the Nile catchment, i.e., in the Sahara, south of the Nile delta. The general enrichment of  $\delta D_{\text{wax } n\text{-alkanoic acid}}$  relative to  $\delta D_{\text{wax } n\text{-alkane}}$  during the early AHP ( $\sim 14.5$ –11 ka; Fig. 4d) provides evidence that the Mediterranean moisture was isotopically heavier than moisture from the Indian and Atlantic oceans, with the latter feeding the African summer monsoonal rainfall (Fig. 1). As such, the reversal to more enriched  $\delta D_{\text{wax } n\text{-alkane}}$  between 11.5–10.5 ka probably attests to increased influence of Mediterranean precipitation in the Sahara and may be indicative of winter rains that extended southward.

The minimum in  $\delta D_{\text{wax } n\text{-alkane}}$  value succeeding the reversal (10.5–7 ka; Fig. 4d) then probably also stems from the amplification of winter precipitation, given the strong

similarity to the minimum in  $\delta D_{\text{wax } n\text{-alkanoic acid}}$  at this time (Fig. 4d). This inference is supported by the absence of comparable minima in  $\delta D_{\text{wax}}$  from lakes Tana, Victoria and Tanganyika (Fig. 4a–c; Berke et al., 2012; Costa et al., 2014; Tierney et al., 2008). Seeking to explain the minimum in  $\delta D_{\text{wax } n\text{-alkane}}$  between 10 and 7 ka, Castañeda et al. (2016a) invoked an eastward shift in the Congo Air Boundary during the AHP optimum, which would enhance the influence of Atlantic moisture over the headwaters. However, the striking similarity between the  $\delta D_{\text{wax } n\text{-alkane}}$  and  $\delta D_{\text{wax } n\text{-alkanoic acid}}$  is a profound argument for the influence of winter precipitation in the Sahara. Acknowledging that  $\delta D_{\text{wax } n\text{-alkane}}$  values remain depleted relative to the  $\delta D_{\text{wax } n\text{-alkanoic acid}}$ , despite the influence of Mediterranean moisture (Fig. 4d), monsoon precipitation probably still substantially influenced the  $\delta D_{\text{wax } n\text{-alkanes}}$  signal. We conclude that the  $\delta D_{\text{wax } n\text{-alkanes}}$  recorded monsoonal precipitation superimposed by Mediterranean winter rainfall during the AHP optimum. As such, we deduce that during this episode, the Mediterranean winter rainfall zone extended southward. Our finding supports earlier studies proposing winter rains that extended southward during the early to mid Holocene in northeastern Africa. South of the Nile delta, the formation of the paleo Faiyum Oasis (Egypt; Fig. 1), which is dated to  $\sim 10$  ka (Hamdan et al., 2016; Hassan et al., 2012), hints at increased winter rains south of the present-day limit of the Mediterranean rainfall zone (i.e., approximately the southern tip of the Nile delta, Cairo). However, the inundation of the Faiyum Depression is, to a large extent, as a result of high Nile floods, which are linked to monsoonal rainfall in the headwaters, and local precipitation is considered to be of minor importance for the lake formation (Hamdan et al., 2016; Wendorf and Schild, 1976; Hassan, 1986). Lacustrine sediments at the northern shore of the modern Quarun Lake, the relict of the paleo Faiyum Oasis, attest to Wadi activity in the region, which is independent of Nile flow and thus indicative of stronger Mediterranean winter rainfall (Hamdan et al., 2020; Koopmann et al., 2016). Moreover, several authors argue that the arrival of East Asian domesticated cereals in the Faiyum region during the early Holocene was enabled by a southward extension of the winter rainfall zone, as most of these crops rely on precipitation to grow in winter and on long daylight hours in summer (Phillipps et al., 2016; Shirai, 2016). Salinity reconstructions from the Red Sea (Arz et al., 2003) and tufa formation on the southern Sinai Peninsula (Hamdan and Brook, 2015) suggest that Mediterranean winter rains reached further south than nowadays.

Cheddadi et al. (2021) proposed that the Mediterranean winter rainfall may have reached as far south as  $18\text{--}24^\circ\text{N}$  over northern Africa, based on a combination of proxy data from Morocco and vegetation modeling. Accordingly, winter rainfall may have played a crucial role in sustaining the green Sahara. Our data confirm that during the AHP optimum an interplay of monsoon (summer) and Mediterranean (winter) rainfall may have existed in the Nile river watershed, which

may have provided the northeastern Sahara with sufficient rainfall throughout the year, allowing plants to occupy the currently barren desert.

## 6 Conclusions

We analyzed  $\delta D_{\text{wax } n\text{-alkanoic acid}}$  in core GeoB7702-3 from the eastern Mediterranean and generated a new continuous record of winter precipitation in the Nile river delta for the past 18 ka in a region where continuous records are sparse. By comparison to previously published records of  $\delta D_{\text{wax } n\text{-alkanes}}$  from the same sediment core, we gain new information about the provenance of leaf wax lipids in the Nile river watershed and about the interplay of Mediterranean (winter) and monsoonal (summer) precipitation around the AHP and their significance for the genesis and sustaining of the green Sahara. Our key findings can be summarized as follows:

1. HMW *n*-alkanoic acids predominantly derived from the delta during the past 18 ka, while the source of the HMW *n*-alkanes varied through time as a function of river runoff and vegetation coverage in the Sahara. Between 15–4 ka, the HMW *n*-alkanes received major contributions from the headwaters and the Sahara once the river runoff was relatively high due to intensified summer rains. Before and after this interval, HMW *n*-alkanes derived from the delta region, like the HMW *n*-alkanoic acids. Around the AHP (14.5–5 ka), the paired application of  $\delta D_{\text{wax } n\text{-alkanoic acid}}$  and  $\delta D_{\text{wax } n\text{-alkane}}$  allows the reconstruction of winter rainfall ( $\delta D_{\text{wax } n\text{-alkanoic acid}}$ ), along with summer monsoonal precipitation ( $\delta D_{\text{wax } n\text{-alkane}}$ ) in the Nile river watershed.
2. HS1 occurred in two phases in the Nile river delta. First, the climate became arid, and wet conditions established at 16 ka. Temperature-induced changes in the precipitation–evaporation balance, as well as variations in the westerly moisture supply, are possible mechanisms. After HS1, the climate remained relatively dry until 11 ka.
3. In the Nile river delta, we find evidence for increased Mediterranean winter rainfall between 11–6 ka, corresponding the optimum of the AHP. Amplified winter precipitation may have resulted from a combination of regional and large-scale factors. Enhanced local cyclogenesis (Cyprus lows) may have been promoted by higher SSTs. Southward-displaced westerlies (negative NAO-like pattern) may be responsible for steering Atlantic storms into the Mediterranean and intensifying the moisture delivery and precipitation in the Nile river delta region. The episode of intensified rainfall was much shorter in the delta region than in the southern Nile catchment, where the summer monsoon

determined precipitation. In the headwaters, the hydroclimate had already begun to ameliorate as early as 14.5 ka.

- At the time of Sahara greening and enhanced precipitation in the delta region (11–6 ka), the monsoonal signal in the  $\delta D_{\text{wax } n\text{-alkane}}$  was superimposed by intensified Mediterranean precipitation in the Sahara. We find proof of concurrently intensified winter and summer precipitation in the Nile river watershed and infer that westerly precipitation was enhanced not only in the delta region but also penetrated farther south into the Sahara. As such, our data support the recently raised hypothesis that monsoonal precipitation, only together with winter precipitation, could allow vegetation to occupy the Sahara desert.

**Data availability.** The data generated in this study are accessible from the PANGAEA database <https://doi.org/10.1594/PANGAEA.961489> (Meyer et al., 2024).

**Supplement.** The supplement related to this article is available online at: <https://doi.org/10.5194/cp-20-523-2024-supplement>.

**Author contributions.** ES designed the study together with VDM, GM and JP. JP provided sediment material for core GeoB7702-3. VDM carried out the sample preparation and analysis in the laboratories and conducted the data processing. ISC and StS analyzed the concentrations of HMW *n*-alkanes. VDM drafted the paper, with contributions from all co-authors.

**Competing interests.** The contact author has declared that none of the authors has any competing interests.

**Disclaimer.** Publisher's note: Copernicus Publications remains neutral with regard to jurisdictional claims made in the text, published maps, institutional affiliations, or any other geographical representation in this paper. While Copernicus Publications makes every effort to include appropriate place names, the final responsibility lies with the authors.

**Acknowledgements.** We thank the captain and the crew of RV *Meteor* for their effort during cruise M52/2. Pushpak Nadar is thanked for his valuable help during processing the biomarker and foraminifera samples in the laboratories at MARUM. Ralph Kreutz is acknowledged for his support during the isotope analysis. We thank Liz Bonk, Hendrik Grotheer and Torben Gentz for their efforts during the AMS measurements. We are grateful to two anonymous reviewers and the editor Christo Buizert for constructive comments during the review process, which helped to improve the quality of the article.

**Financial support.** This research has been supported by the DFG Research Center/Excellence Cluster “The Ocean Floor – Earth’s Uncharted Interface”.

The article processing charges for this open-access publication were covered by the University of Bremen.

**Review statement.** This paper was edited by Christo Buizert and reviewed by two anonymous referees.

## References

- AbuBakr, M., Ghoneim, E., El-Baz, F., Zeneldin, M., and Zeid, S.: Use of radar data to unveil the paleolakes and the ancestral course of Wadi El-Arish, Sinai Peninsula, Egypt, *Geomorphology*, 194, 34–45, <https://doi.org/10.1016/j.geomorph.2013.04.005>, 2013.
- Agrawal, S., Galy, V. V., Sanyal, P., and Eglinton, T. I.: C<sub>4</sub> plant expansion in the Ganga Plain during the last glacial cycle: insights from isotopic composition of vascular plant biomarkers, *Org. Geochem.*, 67, 58–71, <https://doi.org/10.1016/j.orggeochem.2013.12.007>, 2014.
- Almogi-Labin, A., Bar-Matthews, M., Shriki, D., Kolosovsky, E., Paterne, M., Schilman, B., Ayalon, A., Aizenshtat, Z., and Matthews, A.: Climatic variability during the last ~90 ka of the southern and northern Levantine Basin as evident from marine records and speleothems, *Quaternary Sci. Rev.*, 28, 2882–2896, <https://doi.org/10.1016/j.quascirev.2009.07.017>, 2009.
- Alpert, P., Neeman, B., and Shay-El, Y.: Climatological analysis of Mediterranean cyclones using ECMWF data, *Tellus A*, 42, 65–77, <https://doi.org/10.3402/tellusa.v42i1.11860>, 1990.
- Alpert, P., Baldi, M., Ilani, R., Krichak, S., Price, C., Rodó, X., Saaroni, H., Ziv, B., Kishcha, P., Barkan, J., Mariotti, A., and Xoplaki, E.: Relations between climate variability in the Mediterranean region and the tropics: ENSO, South Asian and African monsoons, hurricanes and Saharan dust, *Dev. Earth Environ. Sci.*, 4, 149–177, [https://doi.org/10.1016/S1571-9197\(06\)80005-4](https://doi.org/10.1016/S1571-9197(06)80005-4), 2006.
- AM Online Projects – Alexander Merkel: Climate data for sites worldwide, <https://en.climate-data.org/africa/egypt/cairo-governorate/cairo-3392/>, last access: 14 December 2022a.
- AM Online Projects – Alexander Merkel: Climate data for sites worldwide, <https://en.climate-data.org/africa/egypt/alexandria-governorate/alexandria-515/>, last access: 14 December 2022b.
- AM Online Projects – Alexander Merkel: Climate data for sites worldwide, <https://en.climate-data.org/africa/egypt/luxor-governorate/luxor-6345/>, last access: 14 December 2022c.
- AM Online Projects – Alexander Merkel: Climate data for sites worldwide, <https://en.climate-data.org/africa/ethiopia/addis-ababa/addis-abeba-532/>, last access: 14 December 2022d.
- AM Online Projects – Alexander Merkel: Climate data for sites worldwide, <https://en.climate-data.org/africa/uganda/central-region/kampala-5578/>, last access: 14 December 2022e.
- Arz, H., Lamy, F., Pätzold, J., Müller, P., and Prins, M. A.: Mediterranean moisture source for an Early-Holocene Humid Period in the Northern Red Sea, *Science*, 300, 118–121, <https://doi.org/10.1126/science.1080325>, 2003.

- Bar-Matthews, M., Ayalon, A., and Kaufman, A.: Late Quaternary climate in the eastern Mediterranean region and inferences from the stable isotope systematics of speleothems of the Soreq cave (Israel), *Quaternary Res.*, 47, 155–168, <https://doi.org/10.1006/qres.1997.1883>, 1997.
- Bar-Matthews M., Ayalon A., Kaufman A., and Wasserburg G. J.: The Eastern Mediterranean paleoclimate as a reflection of regional events: Soreq Cave, Israel, *Earth Planet. Sc. Lett.*, 166, 85–95, [https://doi.org/10.1016/S0012-821X\(98\)00275-1](https://doi.org/10.1016/S0012-821X(98)00275-1), 1999.
- Bar-Matthews, M., Ayalon, A., Gilmour, M., Matthews, A., and Hawkesworth, C. J.: Sea – land oxygen isotopic relationships from planktonic foraminifera and speleothems in the Eastern Mediterranean region and their implication for paleorainfall during interglacial intervals, *Geochim. Cosmochim. Ac.*, 67, 3181–3199, [https://doi.org/10.1016/S0016-7037\(02\)01031-1](https://doi.org/10.1016/S0016-7037(02)01031-1), 2003.
- Bartov, Y., Goldstein, S. L., Stein, M., and Enzel, Y.: Catastrophic arid episodes in the Eastern Mediterranean linked with the North Atlantic Heinrich events, *Geology*, 31, 439–442, [https://doi.org/10.1130/0091-7613\(2003\)031<0439:CAEITE>2.0.CO;2](https://doi.org/10.1130/0091-7613(2003)031<0439:CAEITE>2.0.CO;2), 2003.
- Berger, A. and Loutre, M. F.: Insolation values for the climate of the last 10 million years, *Quaternary Sci. Rev.*, 10, 297–317, [https://doi.org/10.1016/0277-3791\(91\)90033-Q](https://doi.org/10.1016/0277-3791(91)90033-Q), 1991.
- Berke, M. A., Johnson, T. C., Werne, J. P., Grice, K., Schouten, S., and Sinninghe Damsté, J. S.: Molecular records of climate variability and vegetation response since the Late Pleistocene in the Lake Victoria basin, East Africa, *Quaternary Sci. Rev.*, 55, 59–74, <https://doi.org/10.1016/j.quascirev.2012.08.014>, 2012.
- Blaauw, M. and Christen, A.: Flexible paleoclimate age-depth models using an autoregressive gamma process, *Bayesian Anal.*, 6, 457–474, <https://doi.org/10.1214/11-BA618>, 2011.
- Blanchet, C., Frank, M., and Schouten, S.: Asynchronous Changes in Vegetation, Runoff and Erosion in the Nile River Watershed during the Holocene, *PLoS One*, 9, 1–18, <https://doi.org/10.1371/journal.pone.0115958>, 2014.
- Blanchet, C. L., Osborne, A. H., Tjallingii, R., Ehrmann, W., Friedrich, T., Timmermann, A., Brückmann, W., and Frank, M.: Drivers of river reactivation in North Africa during the last glacial cycle, *Nat. Geosci.*, 14, 97–103, <https://doi.org/10.1038/s41561-020-00671-3>, 2021.
- Bowen, G. J., Wassenaar, L. I., and Hobson, K. A.: Global application of stable hydrogen and oxygen isotopes to wildlife forensics, *Oecologia*, 143, 337–348, <https://doi.org/10.1007/s00442-004-1813-y>, 2005.
- Braconnot, P., Otto-Bliesner, B., Harrison, S., Joussaume, S., Peterchmitt, J.-Y., Abe-Ouchi, A., Crucifix, M., Driesschaert, E., Fichefet, Th., Hewitt, C. D., Kageyama, M., Kitoh, A., Laine, A., Loutre, M.-F., Marti, O., Merkel, U., Ramstein, G., Valdes, P., Weber, S. L., Yu, Y., and Zhao, Y.: Results of PMIP2 coupled simulations of the Mid-Holocene and Last Glacial Maximum – Part 1: experiments and large-scale features, *Clim. Past*, 3, 261–277, <https://doi.org/10.5194/cp-3-261-2007>, 2007.
- Breitenbach, S. F. M., Adkins, J. F., Meyer, H., Marwan, N., Kumar, K. K., and Haug, G. H.: Strong influence of water vapor source dynamics on stable isotopes in precipitation observed in Southern Meghalaya, NE India, *Earth Planet. Sc. Lett.*, 292, 212–220, <https://doi.org/10.1016/j.epsl.2010.01.038>, 2010.
- Broecker, W. S., McGee, D., Adams, K. D., Cheng, H., Edwards, R. L., Oviatt, C. G., and Quade, J.: A Great Basin-wide dry episode during the first half of the Mystery Interval?, *Quaternary Sci. Rev.*, 28, 2557–2563, <https://doi.org/10.1016/j.quascirev.2009.07.007>, 2009.
- Camberlin, P.: Nile Basin Climates, in: *The Nile*, Springer, 307–333, ISBN 978-1-4020-9725-6, 2009.
- Castañeda, I. S., Schefuß, E., Pätzold, J., Sinninghe Damsté, J. S., Weldeab, S., and Schouten, S.: Millennial-scale sea surface temperature changes in the eastern Mediterranean (Nile River Delta region) over the last 27,000 years, *Paleoceanography*, 25, 1–13, <https://doi.org/10.1029/2009PA001740>, 2010a.
- Castañeda, I. S., Schefuß, E., Pätzold, J., Sinninghe Damsté, J. S., Weldeab, S., and Schouten, S.: (Table 1) Radiocarbon dating of sediment core GeoB7702-3, PANGAEA [data set], <https://doi.org/10.1594/PANGAEA.736913>, 2010b.
- Castañeda, I. S., Schefuß, E., Pätzold, J., Sinninghe Damsté, J. S., Weldeab, S., and Schouten, S.: Isoprenoidal GDGT and alkenone based proxies of sediment core GeoB7702-3, PANGAEA [data set], <https://doi.org/10.1594/PANGAEA.736909>, 2010c.
- Castañeda, I. S., Schouten, S., Pätzold, J., Lucassen, F., Kasemann, S., Kuhlmann, H., and Schefuß, E.: Hydroclimate variability in the Nile River Basin during the past 28,000 years, *Earth Planet. Sc. Lett.*, 438, 47–56, <https://doi.org/10.1016/j.epsl.2015.12.014>, 2016a.
- Castañeda, I. S., Schouten, S., Pätzold, J., Lucassen, F., Kasemann, S. A., Kuhlmann, H., and Schefuß, E.: Organic geochemical analyses of sediment core GeoB7702-3, PANGAEA [data set], [doi.org:10.1594/PANGAEA.858559](https://doi.org/10.1594/PANGAEA.858559), 2016b.
- Chandan, D. and Peltier, W. R.: African humid period precipitation sustained by robust vegetation, soil, and Lake feedbacks, *Geophys. Res. Lett.*, 47, e2020GL088728, <https://doi.org/10.1029/2020GL088728>, 2020.
- Cheddadi, R., Carré, M., Nourelbait, M., François, L., Rhoujjati, A., Manay, R., Ochoa, D., and Schefuß, E.: Early Holocene greening of the Sahara requires Mediterranean winter rainfall, *P. Natl. Acad. Sci. USA*, 118, e2024898118, <https://doi.org/10.1073/pnas.2024898118>, 2021.
- Cheng, H., Sinha, A., Wang, X., Cruz, F. W., and Edwards, R. L.: The Global Paleomonsoon as seen through speleothem records from Asia and the Americas, *Clim. Dynam.*, 39, 1045–1062, <https://doi.org/10.1007/s00382-012-1363-7>, 2012.
- Cheng, H., Sinha A., Verheyden, S., Nader, F. H., Li, X. L., Zhang, P. Z., Yin, J. J., Yi, L., Peng, Y. B., Rao, Z. G., Ning, Y. F., and Edwards, R. L.: The climate variability in northern Levant over the past 20,000 years, *Geophys. Res. Lett.*, 42, 8641–8650, <https://doi.org/10.1002/2015GL065397>, 2015.
- Cheng, H., Lawrence Edwards, R., Sinha, A., Spötl, C., Yi, L., Chen, S., Kelly, M., Kathayat, G., Wang, X., Li, X., Kong, X., Wang, Y., Ning, Y., and Zhang, H.: The Asian monsoon over the past 640,000 years and ice age terminations, *Nature*, 534, 640–646, <https://doi.org/10.1038/nature18591>, 2016.
- Claussen, M., Dallmeyer, A., and Bader, J.: Theory and modeling of the African humid period and the green Sahara, in: *Oxford Research Encyclopedia: Climate Science Vol. 1*, Oxford Research Encyclopedia, Oxford University Press USA, <https://doi.org/10.1093/acrefore/9780190228620.013.532>, 2017.
- Clark, P. U., Dyke, A. S., Shakun, J. D., Carlson, A. E., Clark, J., Wohlfarth, B., Mitrovica, J. X., Hostetler, S. W., and McCabe, A. M.: The Last Glacial Maximum, *Science*, 325, 710–714, <https://doi.org/10.1126/science.1172873>, 2009.

- Collins, J. A., Schefuß, E., Mulitza, S., Prange, M., Werner, M., Tharammal, T., Paul, A., and Wefer, G.: Estimating the hydrogen isotopic composition of past precipitation using leaf-waxes from western Africa, *Quaternary Sci. Rev.*, 65, 88–101, <https://doi.org/10.1016/j.quascirev.2013.01.007>, 2013.
- Collins, J. A., Prange, M., Caley, T., Gimeno, L., Beckmann, B., Mulitza, S., Skonieczny, C., Roche, D., and Schefuß, E.: Rapid termination of the African Humid Period triggered by northern high-latitude cooling, *Nat. Commun.*, 8, 1372, <https://doi.org/10.1038/s41467-017-01454-y>, 2017.
- Columbu, A., Spötl, C., Fohlmeister, J., Hu, H. M., Chiarini, V., Hellstrom, J., Cheng, H., Shen, C. C., and De Waele, J.: Central Mediterranean rainfall varied with high northern latitude temperatures during the last deglaciation, *Commun. Earth Environ.*, 3, 1–9, <https://doi.org/10.1038/s43247-022-00509-3>, 2022.
- Costa, K., Russell, J., Konecky, B., and Lamb, H.: Isotopic reconstruction of the African Humid Period and Congo Air Boundary migration at Lake Tana, Ethiopia, *Quaternary Sci. Rev.*, 83, 58–67, <https://doi.org/10.1016/j.quascirev.2013.10.031>, 2014.
- Dallmeyer, A., Claussen, M., Lorenz, S. J., and Shanahan, T.: The end of the African humid period as seen by a transient comprehensive Earth system model simulation of the last 8000 years, *Clim. Past*, 16, 117–140, <https://doi.org/10.5194/cp-16-117-2020>, 2020.
- De Jonge, C., Stadnitskaia, A., Hopmans, E. C., Cherkashov, G., Fedotov, A., and Sinnighe Damsté, J. S.: In situ produced branched glycerol dialkyl glycerol tetraethers in suspended particulate matter from the Yenisei River, Eastern Siberia, *Geochim. Cosmochim. Ac.*, 125, 476–491, <https://doi.org/10.1016/j.gca.2013.10.031>, 2014.
- deMenocal, P. B.: Palaeoclimate: End of the African humid period, *Nat. Geosci.*, 8, 86–87, <https://doi.org/10.1038/ngeo2355>, 2015.
- deMenocal, P., Ortiz, J., Guilderson, T., Adkins, J., Sarnthein, M., Baker, L., and Yarusinsky, M.: Abrupt onset and termination of the African Humid Period: rapid climate responses to gradual insolation forcing, *Quaternary Sci. Rev.*, 19, 347–361, [https://doi.org/10.1016/S0277-3791\(99\)00081-5](https://doi.org/10.1016/S0277-3791(99)00081-5), 2000a.
- deMenocal P., Ortiz J., Guilderson T., and Sarnthein M.: Coherent high- and low-latitude climate variability during the Holocene warm period, *Science*, 288, 2198–2202, <https://doi.org/10.1126/science.288.5474.2198>, 2000b.
- Dixit, Y., Toucanne, S., Fontanier, C., Pasquier, V., Lora, J. M., Jouet, G., and Tripathi, A.: Enhanced western Mediterranean rainfall during past interglacials driven by North Atlantic pressure changes, *Quaternary Int.*, 553, 1–13, <https://doi.org/10.1016/j.quaint.2020.08.017>, 2020.
- Dupont, L. M. and Schefuß, E.: The roles of fire in Holocene ecosystem changes of West Africa, *Earth Planet. Sc. Lett.*, 481, 255–263, <https://doi.org/10.1016/j.epsl.2017.10.049>, 2018.
- Eglinton, G. and Hamilton, R. J.: Leaf epicuticular waxes, *Science*, 156, 1322–1335, <https://doi.org/10.1126/science.156.3780.1322>, 1967.
- Eglinton, T. I. and Eglinton, G.: Molecular proxies for paleoclimatology, *Earth Planet. Sc. Lett.*, 275, 1–16, <https://doi.org/10.1016/j.epsl.2008.07.012>, 2008.
- Emeis, K. C., Struck, U., Schulz, H. M., Rosenberg, R., Bernasconi, S., Erlenkeuser, H., Sakamoto, T., and Martinez-Ruiz, F.: Temperature and salinity variations of Mediterranean Sea surface waters over the last 16,000 years from records of planktonic stable oxygen isotopes and alkenone unsaturation ratios, *Palaeogeogr. Palaeoclimatol.*, 158, 259–280, [https://doi.org/10.1016/S0031-0182\(00\)00053-5](https://doi.org/10.1016/S0031-0182(00)00053-5), 2000.
- Enzel, Y., Amit, R., Dayan, U., Crouvi, O., Kahana, R., Ziv, B., and Sharon, D.: The climatic and physiographic controls of the eastern Mediterranean over the late Pleistocene climates in the southern Levant and its neighboring deserts, *Global Planet. Change*, 60, 165–192, <https://doi.org/10.1016/j.gloplacha.2007.02.003>, 2008.
- Eshel, G. and Farrel, B. F.: Mechanisms of eastern Mediterranean rainfall variability, *J. Atmos. Sci.*, 57, 3219–32, [https://doi.org/10.1175/1520-0469\(2000\)057<3219:MOEMRV>2.0.CO;2](https://doi.org/10.1175/1520-0469(2000)057<3219:MOEMRV>2.0.CO;2), 2000.
- Fletcher, W. J. and Sanchez Gofii, M. F.: Orbital- and sub-orbital-scale climate impacts on vegetation of the western Mediterranean basin over the last 48,000 yr, *Quaternary Res.*, 70, 451–464, <https://doi.org/10.1016/j.yqres.2008.07.002>, 2008.
- Galy, V. and Eglinton, T.: Protracted storage of biospheric carbon in the Ganges-Brahmaputra basin, *Nat. Geosci.*, 4, 843–847, <https://doi.org/10.1038/ngeo1293>, 2011.
- Gensel, J., Humphries, M. S., Zabel, M., Sebag, D., Hahn, A., and Schefuß, E.: Origin, transport, and retention of fluvial sedimentary organic matter in South Africa's largest freshwater wetland, Mkhuze Wetland System, *Biogeosciences*, 19, 2881–2902, <https://doi.org/10.5194/bg-19-2881-2022>, 2022.
- Giraudi, C., Mercuri, A. M., and Esu, D.: Holocene palaeoclimate in the northern Sahara margin (Jefara Plain, northwestern Libya), *The Holocene*, 23, 339–352, <https://doi.org/10.1177/0959683612460787>, 2013.
- Goldsmith, Y., Polissar, P. J., Ayalon, A., Bar-Matthews, M., deMenocal, P. B., and Broecker, W. S.: The modern and Last Glacial Maximum hydrological cycles of the Eastern Mediterranean and the Levant from a water isotope perspective, *Earth Planet. Sc. Lett.*, 457, 302–312, <https://doi.org/10.1016/j.epsl.2016.10.017>, 2017.
- Häggi, C., Sawakuchi, A. O., Chiessi, C. M., Mulitza, S., Mollenhauer, G., Sawakuchi, H. O., Baker, P. A., Zabel, M., and Schefuß, E.: Origin, transport and deposition of leaf-wax biomarkers in the Amazon Basin and the adjacent Atlantic, *Geochim. Cosmochim. Ac.*, 192, 149–165, <https://doi.org/10.1016/j.gca.2016.07.002>, 2016.
- Hamdan, M. A. and Brook, G. A.: Timing and characteristics of Late Pleistocene and Holocene wetter periods in the Eastern Desert and Sinai of Egypt, based on <sup>14</sup>C dating and stable isotope analysis of spring tufa deposits, *Quaternary Sci. Rev.*, 130, 168–188, <https://doi.org/10.1016/j.quascirev.2015.09.011>, 2015.
- Hamdan, M. A., Flower, R. J., Hassan, F. A., and Leroy, S. A. G.: Geochemical and palynological analysis of Faiyum Lake sediments, Egypt: Implications for Holocene paleoclimate, *J. Afr. Earth Sci.*, 167, 103864, <https://doi.org/10.1016/j.jafrearsci.2020.103864>, 2020.
- Hamdan, M. A., Ibrahim, M. I. A., Shiha, M. A., Flower, R. J., Hassan, F. A., and Eltelet, S. A. M.: An exploratory Early and Middle Holocene sedimentary record with palynofossils and diatoms from Faiyum lake, Egypt, *Quaternary Int.*, 410, 30–42, <https://doi.org/10.1016/j.quaint.2015.12.049>, 2016.
- Hamdan, M. A. and Lucarini, G.: Holocene paleoenvironmental, paleoclimatic and geoarchaeological significance of the Sheikh El-

- Obeiyid area (Farafra Oasis, Egypt), *Quaternary Int.*, 302, 154–168, <https://doi.org/10.1016/j.quaint.2013.01.009>, 2013.
- Hamann, Y., Ehrmann, W., Schmiedl, G., Krüger, S., Stuetz, J. B., and Kuhnt, T.: Sedimentation processes in the Eastern Mediterranean Sea during the Late Glacial and Holocene revealed by end-member modelling of the terrigenous fraction in marine sediments, *Mar. Geol.*, 248, 97–114, <https://doi.org/10.1016/j.margeo.2007.10.009>, 2008.
- Hassan, F. A.: Holocene lakes and prehistoric settlements of the Western Faiyum, Egypt, *J. Archaeol. Sci.*, 13, 483–501, [https://doi.org/10.1016/0305-4403\(86\)90018-X](https://doi.org/10.1016/0305-4403(86)90018-X), 1986.
- Hassan, F. A., Hamdan, M. A., Flower, R. J., and Keatings, K.: Oxygen and carbon isotopic records in Holocene freshwater mollusc shells from the Faiyum palaeolakes, Egypt: Palaeoenvironmental and palaeoclimatic implications, *Quaternary Int.*, 266, 175–187, <https://doi.org/10.1016/j.quaint.2011.11.024>, 2012.
- Heaton, T. J., Köhler, P., Butzin, M., Bard, E., Reimer, R. W., Austin, W. E. N., Bronk Ramsey, C., Grootes, P. M., Hughen, K. A., Kromer, B., Reimer, P. J., Adkins, J., Burke, A., Cook, M. S., Olsen, J., and Skinner, L. C.: Marine20 – The Marine Radiocarbon Age Calibration Curve (0–55,000 cal. BP), *Radiocarbon*, 62: IntCal20: Calibration Issue, 779–820, <https://doi.org/10.1017/RDC.2020.68>, 2020.
- Hedges, J. I., Keil, R. G., and Benner, R.: What happens to terrestrial organic matter in the ocean?, *Org. Geochem.*, 27, 195–212, [https://doi.org/10.1016/S0146-6380\(97\)00066-1](https://doi.org/10.1016/S0146-6380(97)00066-1), 1997.
- Hély, C., Lézine, A.-M., and contributors, A.: Holocene changes in African vegetation: tradeoff between climate and water availability, *Clim. Past*, 10, 681–686, <https://doi.org/10.5194/cp-10-681-2014>, 2014.
- Hemingway, J. D., Schefuß, E., Dinga, B. J., Pryer, H., and Galy, V. V.: Multiple plant-wax compounds record differential sources and ecosystem structure in large river catchments, *Geochim. Cosmochim. Acta*, 184, 20–40, <https://doi.org/10.1016/j.gca.2016.04.003>, 2016.
- Hoefs, M. J. L., Rijpstra, W. I. C., and Sinninghe Damste, J. S.: The influence of oxic degradation on the sedimentary biomarker record I: evidence from Madeira Abyssal Plain turbidites, *Geochim. Cosmochim. Acta*, 66, 2719–2735, [https://doi.org/10.1016/S0016-7037\(02\)00864-5](https://doi.org/10.1016/S0016-7037(02)00864-5), 2002.
- Hopcroft, P. O., Valdes, P. J., Harper, A. B., and Beerling, D. J.: Multi vegetation model evaluation of the green Sahara climate regime, *Geophys. Res. Lett.*, 44, 6804–6813, <https://doi.org/10.1002/2017GL073740>, 2017.
- Jolly, D., Prentice, I. C., Bonnefille, R., Ballouche, A., Bengo, M., Brenac, P., Buchet, G., Burney, D., Cazet, J. P., Cheddadi, R., Ederh, T., Elenga, H., Elmoutaki, S., Guiot, J., Laarif, F., Lamb, H., Lezine, A. M., Maley, J., Mbenza, M., Peyron, O., Reille, M., Reynaud-Farrera, I., Riollet, G., Ritchie, J. C., Roche, E., Scott, L., Ssemmanda, I., Straka, H., Umer, M., Van Campo, E., Vili-mumbalo, S., Vincens, A., and Waller, M.: Biome reconstruction from pollen and plant macrofossil data for Africa and the Arabian peninsula at 0 and 6000 years, *J. Biogeogr.*, 25, 1007–1027, <https://doi.org/10.1046/j.1365-2699.1998.00238.x>, 1998.
- Junginger, A., Roller, S., Olaka, L. A., and Trauth, M. H.: The effects of solar irradiation changes on the migration of the Congo Air Boundary and water levels of paleo-Lake Suguta, Northern Kenya Rift, during the African Humid Period (15–5 ka BP), *Palaeogeogr. Palaeoclimatol.*, 396, 1–16, <https://doi.org/10.1016/j.palaeo.2013.12.007>, 2014.
- Kageyama, M., Harrison, S. P., Kapsch, M.-L., Lofverstrom, M., Lora, J. M., Mikolajewicz, U., Sherriff-Tadano, S., Vadsaria, T., Abe-Ouchi, A., Bouttes, N., Chandan, D., Gregoire, L. J., Ivanovic, R. F., Izumi, K., LeGrande, A. N., Lhardy, F., Lohmann, G., Morozova, P. A., Ohgaito, R., Paul, A., Peltier, W. R., Poulsen, C. J., Quiquet, A., Roche, D. M., Shi, X., Tierney, J. E., Valdes, P. J., Volodin, E., and Zhu, J.: The PMIP4 Last Glacial Maximum experiments: preliminary results and comparison with the PMIP3 simulations, *Clim. Past*, 17, 1065–1089, <https://doi.org/10.5194/cp-17-1065-2021>, 2021.
- Konecky, B. L., Russell, J. M., Johnson, T. C., Brown, E. T., Berke, M. A., Werne, J. P., and Huang, Y.: Atmospheric circulation patterns during late Pleistocene climate changes at Lake Malawi, Africa, *Earth Planet. Sc. Lett.*, 312, 318–326, <https://doi.org/10.1016/j.epsl.2011.10.020>, 2011.
- Koopman, A., Kluiving, S., Holdaway, S., and Wendrich, W.: The Effects of Holocene Landscape Changes on the Formation of the Archaeological Record in the Fayum Basin, Egypt, *Geoarchaeology*, 31, 17–33, <https://doi.org/10.1002/gea.21538>, 2016.
- Korecha, D. and Barnston, A. G.: Predictability of June–September Rainfall in Ethiopia, *Mon. Weather Rev.*, 135, 628–650, <https://doi.org/10.1175/MWR3304.1>, 2007.
- Krichak, S. O., Breitgand, J. S., and Feldstein, S. B.: A conceptual model for the identification of active Red Sea Trough synoptic events over the south-eastern Mediterranean, *J. Appl. Meteorol. Clim.*, 51, 962–71, <https://doi.org/10.1175/JAMC-D-11-0223.1>, 2012.
- Krom, M. D., Cliff, R. A., Eijssink, L. M., Herut, B., and Chester, R.: The characterisation of Saharan dusts and Nile particulate matter in surface sediments from the Levantine basin using Sr isotopes, *Mar. Geol.*, 155, 319–330, [https://doi.org/10.1016/S0025-3227\(98\)00130-3](https://doi.org/10.1016/S0025-3227(98)00130-3), 1999.
- Kuper, R. and Kröpelin, S.: Climate-controlled Holocene occupation in the Sahara: Motor of Africa’s evolution, *Science*, 313, 803–807, <https://doi.org/10.1126/science.1130989>, 2006.
- Kusch, S., Rethemeyer, J., Schefuß, E., and Mollenhauer, G.: Controls on the age of vascular plant biomarkers in Black Sea sediments, *Geochim. Cosmochim. Acta*, 74, 7031–7047, <https://doi.org/10.1016/j.gca.2010.09.005>, 2010.
- Kutzbach, J. E., Chen, G., Cheng, H., Edwards, R. L., and Liu, Z.: Potential role of winter rainfall in explaining increased moisture in the Mediterranean and Middle East during periods of maximum orbitally-forced insolation seasonality, *Clim. Dynam.*, 42, 1079–1095, <https://doi.org/10.1007/s00382-013-1692-1>, 2014.
- Lamb, H. F., Bates, C. R., Coombes, P. V., Marshall, M. H., Umer, M., Davies, S. J., and Dejen, E.: Late Pleistocene desiccation of Lake Tana, source of the Blue Nile, *Quaternary Sci. Rev.*, 26, 287–299, <https://doi.org/10.1016/j.quascirev.2006.11.020>, 2007.
- Langgut, D., Cheddadi, R., and Sharon, G.: Climate and environmental reconstruction of the Epipaleolithic Mediterranean Levant (22.0–11.9 ka cal. BP), *Quaternary Sci. Rev.*, 270, 107170, <https://doi.org/10.1016/j.quascirev.2021.107170>, 2021.
- Larrasoana, J. C., Roberts, A. P., and Rohling, E. J.: Dynamics of Green Sahara Periods and Their Role in Hominin Evolution, *PLoS One*, 8, e76514, <https://doi.org/10.1371/journal.pone.0076514>, 2013.

- Lenderink, G. and Meijgaard, E. V.: Increase in hourly precipitation extremes beyond expectations from temperature changes, *Nat. Geosci.*, 1, 511–514, <https://doi.org/10.1038/ngeo262>, 2008.
- Li, Y., Song, Y., Yin, Q., Han, L., and Wang, Y.: Orbital and millennial northern mid-latitude westerlies over the last glacial period, *Clim. Dynam.*, 53, 3315–3324, <https://doi.org/10.1007/s00382-019-04704-5>, 2019.
- Lisiecki, L. E. and Raymo, M. E.: A Pliocene-Pleistocene stack of 57 globally distributed benthic  $\delta^{18}\text{O}$  records, *Paleoceanography*, 20, PA1003, <https://doi.org/10.1029/2004PA001071>, 2005.
- Löffverström, M. and Lora, J. M.: Abrupt regime shifts in the North Atlantic atmospheric circulation over the last deglaciation, *Geophys. Res. Lett.*, 44, 8047–8055, <https://doi.org/10.1002/2017GL074274>, 2017.
- Ludwig, P. and Hochman, A.: Last glacial maximum hydroclimate and cyclone characteristics in the Levant: A regional modelling perspective, *Environ. Res. Lett.*, 17, 014053, <https://doi.org/10.1088/1748-9326/ac46ea>, 2022.
- Lüning, S. and Vahrenholt, F.: Holocene Climate Development of North Africa and the Arabian Peninsula, in: *The Geology of the Arab World – An Overview*, edited by: Bendaoud, A., Hamimi, Z., Hamoudi, M., Djemai, S., and Zoheir, B., Springer Geology, 507–546, <https://doi.org/10.1007/978-3-319-96794-3>, 2019.
- Martin, C., Ménot, G., Thouveny, N., Davtian, N., Andrieu-Ponel, V., Reille, M., and Bard, E.: Impact of human activities and vegetation changes on the tetraether sources in Lake St Front (Massif Central, France), *Org. Geochem.*, 135, 38–52, <https://doi.org/10.1016/j.orggeochem.2019.06.005>, 2019.
- Marshall, M. H., Lamb, H. F., Huws, D., Davies, S. J., Bates, R., Bloemendal, J., Boyle, J., Leng, M. J., Umer, M., and Bryant, C.: Late Pleistocene and Holocene drought events at Lake Tana, the source of the Blue Nile, *Glob. Planet. Change*, 78, 147–161, <https://doi.org/10.1016/j.gloplacha.2011.06.004>, 2011.
- Ménot, G., Pivot, S., Bouloubassi, I., Davtian, N., Hennekam, R., Bosch, D., Ducassou, E., Bard, E., Migeon, S., and Revel, M.: Timing and stepwise transitions of the African Humid Period from geochemical proxies in the Nile deep-sea fan sediments, *Quaternary Sci. Rev.*, 228, 106071, <https://doi.org/10.1016/j.quascirev.2019.106071>, 2020.
- Menviel, L., Govin, A., and Grant, K. M.: Drivers of the evolution and amplitude of African Humid Periods, *Commun. Earth Environ.*, 2, 237, <https://doi.org/10.1038/s43247-021-00309-1>, 2021.
- Meyer, V. D., Pätzold, J., Mollenhauer, G., Castañeda, I. S., Schouten, S., Schefuß, E.: Radiocarbon dates, biomarker concentrations and compound-specific isotopes data of sediment core GeoB7702-3, PANGAEA [data set], <https://doi.org/10.1594/PANGAEA.961489>, 2024.
- Meyers, P. A. and Ishiwatari, R.: Lacustrine organic geochemistry – an overview of indicators of organic matter sources and diagenesis in lake sediments, *Org. Geochem.*, 20, 867–900, [https://doi.org/10.1016/0146-6380\(93\)90100-P](https://doi.org/10.1016/0146-6380(93)90100-P), 1993.
- Miebach, A., Stolzenberger, S., Wacker, L., Hense, A., and Litt, T.: A new Dead Sea pollen record reveals the last glacial paleoenvironment of the southern Levant, *Quaternary Sci. Rev.*, 214, 98–116, <https://doi.org/10.1016/j.quascirev.2019.04.033>, 2019.
- Mollenhauer, G., Grotheer, H., Gentz, T., Bonk, E., and Hefter, J.: Standard operation procedures and performance of the MICADAS radiocarbon laboratory at Alfred Wegener Institute (AWI), Germany, *Nucl. Instrum. Methods*, 496, 45–51, <https://doi.org/10.1016/j.nimb.2021.03.016>, 2021.
- Muhs, D. R., Roskin, J., Tsoar, H., Skipp, G., Budahn, J. R., Sneh, A., Porat, N., Stanley, J. D., Katra, I., and Blumberg, D. G.: Origin of the Sinai-Negev erg, Egypt and Israel: Mineralogical and geochemical evidence for the importance of the Nile and sea level history, *Quaternary Sci. Rev.*, 69, 28–48, <https://doi.org/10.1016/j.quascirev.2013.02.022>, 2013.
- Naughton, F., Sánchez Goñi, M. F., Kageyama, M., Bard, E., Cortijo, E., Desprat, S., Malaizé, B., Joly, C., Rostek, F., and Turon, J.-L.: Wet to dry climatic trend in north western Iberia within Heinrich events, *Earth Planet. Sc. Lett.*, 284, 329–342, <https://doi.org/10.1016/j.epsl.2009.05.001>, 2009.
- Naughton, F., Sanchez Goñi, M. F., Rodrigues, T., Salgueiro, E., Costas, S., Desprat, S., Duprat, J., Michel, E., Rossignol, L., Zaragosi, S., Voelker, A. H. L., and Abrantes, F.: Climate variability across the last deglaciation in NW Iberia and its margin, *Quaternary Int.*, 414, 9–22, <https://doi.org/10.1016/j.quaint.2015.08.073>, 2016.
- Naughton, F., Toucanne, S., Landais, A., Rodrigues, T., Vazquez Riveiros, N., and Sánchez-Goñi, M. F.: Chapter 5 – Heinrich Stadial 1, in: *European Glacial Landscapes – The Last Deglaciation*, edited by: Palacios, D., Hughes, P. D., García-Ruiz, J. M., and Andrés N., Elsevier, 37–44, ISBN 9780323918992, [doi.org/10.1016/B978-0-323-91899-2.00049-8](https://doi.org/10.1016/B978-0-323-91899-2.00049-8), 2023.
- Otto-Bliesner, B. L., Russell, J. M., Clark, P. U., Liu, Z., Overpeck, J. T., Konecky, B., Nicholson, S. E., He, F., and Lu, Z.: Coherent changes of southeastern equatorial and northern African rainfall during the last deglaciation, *Science*, 346, 1223–1227, <https://doi.org/10.1126/science.1259531>, 2014.
- Palchan, D. and Torfstein, A.: A drop in Sahara dust fluxes records the northern limits of the African Humid Period, *Nat. Commun.*, 10, 3803, <https://doi.org/10.1038/s41467-019-11701-z>, 2019.
- Pausata, F. S. R., Messori, G., and Zhang, Q.: Impacts of dust reduction on the northward expansion of the African monsoon during the green Sahara period, *Earth Planet. Sc. Lett.*, 434, 298–307, <https://doi.org/10.1016/j.epsl.2015.11.049>, 2016.
- Pausata, F. S. R., Gaetani, M., Messori, G., Berg, A., Maia de Souza, D., Sage, R. F., and deMenocal, P. B.: The greening of the Sahara: Past changes and future implications, *One Earth*, 2, 235–250, <https://doi.org/10.1016/j.oneear.2020.03.002>, 2020.
- Pätzold, J., Bohrmann, G., and Hübscher, C.: Black Sea – Mediterranean – Red Sea. Cruise No. 52, 2 January–27 March 2002, Istanbul – Limassol, Universität Hamburg, METEOR-Berichte 3–2, 178 pp., [https://doi.org/10.3289/GEOMAR\\_REP\\_108\\_2002](https://doi.org/10.3289/GEOMAR_REP_108_2002), 2003.
- Pérez-Mejías, C., Moreno, A., Bernal-Wormull, J., Cacho, I., Osácar, M. C., Lawrence, E., and Chang, E.: Oldest Dryas hydroclimate reorganization in the eastern Iberian Peninsula after the iceberg discharges of Heinrich Event 1, *Quaternary Res.*, 101, 67–83, <https://doi.org/10.1017/qua.2020.112>, 2021.
- Perez-Sanz, A., Li, G., González-Sampérez, P., and Harrison, S. P.: Evaluation of modern and mid-Holocene seasonal precipitation of the Mediterranean and northern Africa in the CMIP5 simulations, *Clim. Past*, 10, 551–568, <https://doi.org/10.5194/cp-10-551-2014>, 2014.
- Phillipps, R., Holdaway, S., Ramsay, R., Emmitt, J., Wendrich, W., and Linseele, V.: Lake level changes, lake edge basins and the paleoenvironment of the Fayum North shore, Egypt,

- during the early to mid-Holocene, *Open Quat.*, 2, 1–12, <https://doi.org/10.5334/oq.19>, 2016.
- Quade, J., Dente, E., Armon, M., Ben Dor, Y., Morin, E., Adam, O., and Enzel, Y.: Megalakes in the Sahara? A Review, *Quaternary Res.*, 90, 253–275, <https://doi.org/10.1017/qua.2018.46>, 2018.
- Reimer, P. J. and Reimer, R. W.: A marine reservoir correction database and on-line interface, *Radiocarbon*, 43, 461–463, <https://doi.org/10.1017/S0033822200038339>, 2001.
- Revel, M., Ducassou, E., Grousset, F. E., Bernasconi, S. M., Migeon, S., Revillon, S., Mascle, J., Murat, A., Zaragosi, S., and Bosch, D.: 100,000 Years of African monsoon variability recorded in sediments of the Nile margin, *Quaternary Sci. Rev.*, 29, 1342–1362, <https://doi.org/10.1016/j.quascirev.2010.02.006>, 2010.
- Revel, M., Colin, C., Bernasconi, S., Combourieu-Nebout, N., Ducassou, E., Grousset, F. E., Rolland, Y., Migeon, S., Bosch, D., Brunet, P., Zhao, Y., and Mascle, J.: 21,000 years of Ethiopian African monsoon variability recorded in sediments of the western Nile deep-sea fan, *Reg. Environ. Change*, 14, 1685–1696, <https://doi.org/10.1007/s10113-014-0588-x>, 2014.
- Revel, M., Ducassou, E., Skonieczny, C., Colin, C., Bastian, L., Bosch, D., Migeon, S., and Mascle, J.: 20,000 years of Nile River dynamics and environmental changes in the Nile catchment area as inferred from Nile upper continental slope sediments, *Quaternary Sci. Rev.*, 130, 200–221, <https://doi.org/10.1016/j.quascirev.2015.10.030>, 2015.
- Ruan, Y., Mohtadi, M., van der Kaas, S., Dupont, L. M., Hebbeln, D., and Schefuß, E.: Differential hydroclimatic evolution of East Javanese ecosystems over the past 22,000 years, *Quaternary Sci. Rev.*, 218, 49–60, <https://doi.org/10.1016/j.quascirev.2019.06.015>, 2019.
- Sachse, D., Billault, I., Bowen, G. J., Chikaraishi, Y., Dawson, T. E., Feakins, S. J., Freeman, K. H., Magill, C. R., McInerney, F. A., van der Meer, M. T. J., Polissar, P., Robins, R. J., Sachs, J. P., Schmidt, H.-L., Sessions, A. L., White, J. W. C., West, J. B., and Kahmen, A.: Molecular paleohydrology: interpreting the hydrogen-isotopic composition of lipid biomarkers from photosynthesizing organisms, *Annu. Rev. Earth Pl. Sc.*, 40, 221–249, <https://doi.org/10.1146/annurev-earth-042711-105535>, 2012.
- Schefuß, E., Schouten, S., and Schneider, R. R.: Climatic controls on central African hydrology during the past 20,000 years, *Nature*, 437, 1003–1006, <https://doi.org/10.1038/nature03945>, 2005.
- Schlitzer, R.: Ocean Data View v.5.6.3, Alfred Wegener Institute [code], <https://odv.awi.de/> (last access: 5 January 2023), 2006.
- Schlünz, B. and Schneider, R. R.: Transport of terrestrial organic carbon to the oceans by rivers: re-estimating flux- and burial rates, *Int. J. Earth Sci.*, 88, 599–606, 2000.
- Schreuder, L. T., Stuut, J.-B. W., Korte, L. F., Sinninghe Damsté, J. S., and Schouten, S.: Aeolian transport and deposition of plant wax *n*-alkanes across the tropical North Atlantic Ocean, *Org. Geochem.*, 115, 113–123, <https://doi.org/10.1016/j.orggeochem.2017.10.010>, 2018.
- Sha, L., Ait Brahim, Y., Wassenburg, J. A., Yin, J., Peros, M., Cruz, F. W., Cai, Y., Li, H., Du, W., Zhang, H., Edwards, R. L., and Cheng, H.: How Far North Did the African Monsoon Fringe Expand During the African Humid Period? Insights From Southwest Moroccan Speleothems, *Geophys. Res. Lett.*, 46, 14093–14102, <https://doi.org/10.1029/2019GL084879>, 2019.
- Shanahan, T. M., Mckay, N. P., Hughen, K. A., Overpeck, J. T., Otto-Bliesner, B., Heil, C. W., King, J., Scholz, C. A., and Peck, J.: The time-transgressive termination of the African humid period, *Nat. Geosci.*, 8, 140–144, <https://doi.org/10.1038/ngeo2329>, 2015.
- Shirai, N.: Establishing a Neolithic farming life in Egypt: A view from the lithic study at Fayum Neolithic sites, *Quatern. Int.*, 412, 22–35, <https://doi.org/10.1016/j.quaint.2015.10.111>, 2016.
- Sinninghe Damsté, J. S., Rijpstra, W. I. C., and Reichert, G.-J.: The influence of oxic degradation on the sedimentary biomarker record II. Evidence from Arabian Sea sediments, *Geochim. Cosmochim. Ac.*, 66, 2737–2754, [https://doi.org/10.1016/S0016-7037\(02\)00865-7](https://doi.org/10.1016/S0016-7037(02)00865-7), 2002.
- Stager, J. C., Ryves, D. B., Chase, B. M., and Pausata, F. S.: Catastrophic drought in the Afro-Asian monsoon region during Heinrich event 1, *Science*, 331, 1299–1302, <https://doi.org/10.1126/science.1198322>, 2011.
- Stein, M.: The sedimentary and geochemical record of Neogene-Quaternary water bodies in the Dead Sea basin – inferences for the regional paleoclimate history, *J. Paleolimnol.*, 26, 271–282, <https://doi.org/10.1023/A:1017529228186>, 2001.
- Stein, M., Starinsky, A., Katz, A., Goldstein, S., Machlus, M., and Schramm, A.: Strontium isotopic, chemical, and sedimentological evidence for the evolution of Lake Lisan and the Dead Sea, *Geochim. Cosmochim. Ac.*, 61, 3975–3992, [https://doi.org/10.1016/S0016-7037\(97\)00191-9](https://doi.org/10.1016/S0016-7037(97)00191-9), 1997.
- Stockhecke, M., Timmermann, A., Kipfer, R., Haug, G. H., Kwiecien, O., Friedrich, T., Menviel, L., Litt, T., Pickarski, N., and Anselmetti, F. S.: Millennial to orbital-scale variations of drought intensity in the Eastern Mediterranean, *Quaternary Sci. Rev.* 133, 77–95, <https://doi.org/10.1016/j.quascirev.2015.12.016>, 2016.
- Tierney, J. E., Russell, J. M., Huang, Y., Sinninghe Damsté, J. S., Hopmans, E. C., and Cohen, A. S.: Northern hemisphere controls on tropical southeastern African climate during the past 60,000 years, *Science*, 322, 252–255, <https://doi.org/10.1126/science.1160485>, 2008.
- Thompson, A. J., Skinner, C. B., Poulsen, C. J., and Zhu, J.: Modulation of Mid-Holocene African Rainfall by Dust Aerosol Direct and Indirect Effects, *Geophys. Res. Lett.*, 46, 3917–3926, <https://doi.org/10.1029/2018GL081225>, 2019.
- Thompson, A. J., Tabor, C. R., Poulsen, C. J., and Skinner, C. B.: Water isotopic constraints of the mid-Holocene West African Monsoon, *EPSL*, 554, 11667, <https://doi.org/10.1016/j.epsl.2020.116677>, 2021.
- Tierney, J. E. and de Menocal, P. B.: Abrupt shifts in Horn of Africa hydroclimate since the Last Glacial Maximum, *Science*, 342, 843–846, <https://doi.org/10.1126/science.1240411>, 2013.
- Tierney, J. E., Russell, J. M., and Huang, Y.: A molecular perspective on Late Quaternary climate and vegetation change in the Lake Tanganyika basin, East Africa, *Quaternary Sci. Rev.*, 29, 787–800, <https://doi.org/10.1016/j.quascirev.2009.11.030>, 2010.
- Tierney, J. E., Pausata, F. S. R., and deMenocal, P. B.: Rainfall regimes of the Green Sahara, *Sci. Adv.*, 3, 1–10, <https://doi.org/10.1126/sciadv.1601503>, 2017.
- Tierney, J. E., Torfstein, A., and Bhattacharya, T.: Late Quaternary hydroclimate of the Levant: The leaf wax record from the Dead Sea, *Quaternary Sci. Rev.*, 289, 107613, <https://doi.org/10.1016/j.quascirev.2022.107613>, 2022.

- Tsvieli, Y. and Zangvil, A.: Synoptic climatological analysis of the “wet” and “dry” Red Sea troughs over Israel, *Int. J. Climatol.*, 25, 1997–2015, <https://doi.org/10.1002/joc.1232>, 2005.
- Trenberth, K. E., Dai, A., Rasmussen, R. M., and Parsons, D. B.: The changing character of precipitation, *B. Am. Meteorol. Soc.*, 84, 1205–1217, <https://doi.org/10.1175/BAMS-84-9-1205>, 2003.
- Valsecchi, V., Sanchez Goñi, M. F., and Londeix, L.: Vegetation dynamics in the Northeastern Mediterranean region during the past 23 000 yr: insights from a new pollen record from the Sea of Marmara, *Clim. Past*, 8, 1941–1956, <https://doi.org/10.5194/cp-8-1941-2012>, 2012.
- Viste, E. and Sorteberg, A.: The effect of moisture transport variability on Ethiopian summer precipitation, *Int. J. Climatol.*, 33, 3106–3123, <https://doi.org/10.1002/joc.3566>, 2013.
- Wagner, B., Vogel, H., Francke, A., Friedrich, T., Donders, T., Lacey, J. H., Leng, M. J., Regattieri, E., Sadori, L., Wilke, T., Zanchetta, G., Albrecht, C., Bertini, A., Combourieu-Nebout, N., Cvetkoska, A., Giaccio, B., Grazhdani, A., Hauffe, T., Holtvoeth, J., Joannin, S., Jovanovska, E., Just, J., Kouli, K., Kousis, I., Koutsodendris, A., Krastel, S., Lagos, M., Leicher, N., Levkov, Z., Lindhorst, K., Masi, A., Melles, M., Mercuri, A. M., Nomade, S., Nowaczyk, N., Panagiotopoulos, K., Peyron, O., Reed, J. M., Sagnotti, L., Sinopoli, G., Stelbrink, B., Sulpizio, R., Timmermann, A., Tofilovska, S., Torri, P., Wagner-Cremer, F., Wonik, T., and Zhang, X.: Mediterranean winter rainfall in phase with African monsoons during the past 1.36 million years, *Nature*, 573, 256–260, <https://doi.org/10.1038/s41586-019-1529-0>, 2019.
- Wang, N., Jiang, D., and Lang, X.: Northern westerlies during the last glacial maximum: Results from CMIP5 simulations, *J. Climate*, 31, 1135–1153, <https://doi.org/10.1175/JCLI-D-17-0314.1>, 2018.
- Wassenburg, J. A., Dietrich, S., Fietzke, J., Fohlmeister, J., Jochum, K. P., Scholz, D., Richter, D. K., Sabouhi, A., Spötl, C., Lohmann, G., Andreae, M. O., and Immenhauser, A.: Reorganization of the North Atlantic Oscillation during early Holocene deglaciation, *Nat. Geosci.*, 9, 602–605, <https://doi.org/10.1038/ngeo2767>, 2016.
- Watrin, J., Lézine, A. M., Hély, C., Cour, P., Ballouche, A., Duzer, D., Elenga, H., Frédoux, A., Guinet, P., Jahns, S., Kadomura, H., Maley, J., Mercuri, A. M., Pons, I. A., Reynaud-Farrera, I., Ritchie, J. C., Salzmann, U., Schulz, E., Tossou, M. G., Vincens, A., and Waller, M. P.: Plant migration and plant communities at the time of the “green Sahara”, *CR Geosci.*, 341, 656–670, <https://doi.org/10.1016/j.crte.2009.06.007>, 2009.
- Weijers, J. W. H., Schouten, S., Hopmans, E. C., Geenevasen, J. A. J., David, O. R. P., Coleman, J. M., Pancost, R. D., and Sinninghe Damsté, J. S.: Membrane lipids of mesophilic anaerobic bacteria thriving in peats have typical archaeal traits, *Environ. Microbiol.*, 8, 648–657, <https://doi.org/10.1111/j.1462-2920.2005.00941.x>, 2006.
- Weldeab, S., Emeis, K.-C., Hemleben, C., and Siebel, W.: Provenance of lithogenic surface sediments and pathways of riverine suspended matter in the Eastern Mediterranean Sea: evidence from  $^{143}\text{Nd} / ^{144}\text{Nd}$  and  $^{87}\text{Sr} / ^{86}\text{Sr}$  ratios, *Chem. Geol.*, 186, 139–149, [https://doi.org/10.1016/S0009-2541\(01\)00415-6](https://doi.org/10.1016/S0009-2541(01)00415-6), 2002.
- Weldeab, S., Menke, V., and Schmiedl, G.: The pace of East African monsoon evolution during the Holocene, *Geophys. Res. Lett.*, 41, 1724–1732, <https://doi.org/10.1002/2014GL059361>, 2014.
- Wendorf, F. and Schild, R.: *Prehistory of the Nile Valley*, Academic Press, London, ISBN 0127439501, 1976.
- Williams, M., Talbot, M., Aharon, P., Abdl Salaam, Y., Williams, F., and Inge Brendeland, K.: Abrupt return of the summer monsoon 15,000 years ago: new supporting evidence from the lower White Nile valley and Lake Albert, *Quaternary Sci. Rev.*, 25, 2651–2665, <https://doi.org/10.1016/j.quascirev.2005.07.019>, 2006.
- Williams, M. A. J.: Late Pleistocene and Holocene environments in the Nile basin, *Global Planet. Change*, 69, 1–15, <https://doi.org/10.1016/j.gloplacha.2009.07.005>, 2009.
- Williams, M. A. J., Usai, D., Salvatori, S., Williams, F. M., Zerbini, A., Maritan, L., and Linseele, V.: Late Quaternary environments and prehistoric occupation in the lower White Nile valley, central Sudan, *Quaternary Sci. Rev.*, 130, 72–88, <https://doi.org/10.1016/j.quascirev.2015.03.007>, 2015.
- Zaki, A. S., King, G. E., Haghypour, N., Giegengack, R., Watkins, S. E., Gupta, S., Schuster, M., Khairy, H., Ahmed, S., El-Wakil, M., Eltayeb, S. A., Herman, F., and Castelltort, S.: Did increased flooding during the African Humid Period force migration of modern humans from the Nile Valley?, *Quaternary Sci. Rev.*, 272, 107200, <https://doi.org/10.1016/j.quascirev.2021.107200>, 2021.
- Ziegler, M., Tuenter, E., and Lourens, L.: The precession phase of the boreal summer monsoon as viewed from the eastern Mediterranean (ODP Site 968), *Quaternary Sci. Rev.*, 29, 1481–1490, <https://doi.org/10.1016/j.quascirev.2010.03.011>, 2010.